



저작자표시-비영리-변경금지 2.0 대한민국

이용자는 아래의 조건을 따르는 경우에 한하여 자유롭게

- 이 저작물을 복제, 배포, 전송, 전시, 공연 및 방송할 수 있습니다.

다음과 같은 조건을 따라야 합니다:



저작자표시. 귀하는 원저작자를 표시하여야 합니다.



비영리. 귀하는 이 저작물을 영리 목적으로 이용할 수 없습니다.



변경금지. 귀하는 이 저작물을 개작, 변형 또는 가공할 수 없습니다.

- 귀하는, 이 저작물의 재이용이나 배포의 경우, 이 저작물에 적용된 이용허락조건을 명확하게 나타내어야 합니다.
- 저작권자로부터 별도의 허가를 받으면 이러한 조건들은 적용되지 않습니다.

저작권법에 따른 이용자의 권리는 위의 내용에 의하여 영향을 받지 않습니다.

이것은 [이용허락규약\(Legal Code\)](#)을 이해하기 쉽게 요약한 것입니다.

[Disclaimer](#)

이학석사 학위논문

Biogeochemical studies of
greenhouse gas formation from
two ice complexes of Batagay
Megaslump, East Siberia

동시베리아 바타가이 메가슬럼프의 두
얼음층에서의 온실기체 형성에 관한 생지화학적
연구

2023년 8월

서울대학교 대학원
지구환경과학부
박 한 수

Biogeochemical studies of greenhouse gas formation from two ice complexes of Batagay Megaslump, East Siberia

Adviser Jinho Ahn

Submitting a master' s thesis of
Science in Earth and Environmental Sciences

May 2023

Graduate School of Natural Sciences
Seoul National University
Earth and Environmental Sciences Major

Hansu Park

Confirming the master' s thesis written by

Hansu Park

July 2023

Chair _____ (Seal)

Vice Chair _____ (Seal)

Examiner _____ (Seal)

Abstract

Permafrost can be a significant source of greenhouse gases (GHGs) under global warming in the future. However, the source and control mechanisms of GHGs in permafrost regions are not well understood. Ice wedges, commonly found in subsurface permafrost regions, contain gas bubbles with very high concentration of GHGs. Analysis of GHGs in the gas bubbles may help us better understand control mechanisms of GHG formation at subzero temperature in permafrost regions. The Batagay megaslump, which is located in the Yana Highlands of northern Yakutia, is the largest thaw slump in the world. Here, I used ice-wedge samples from two stratigraphic units: the Upper Ice Complex (UIC) and the Lower Ice Complex (LIC) of the Batagay megaslump. I estimated the ice-wedge formation processes by analyzing the Ar/N₂/O₂ compositions of the gas bubble and stable water isotopic ratios ($\delta^{18}\text{O}$ and δD) of the wedge ice. Then, the sources and control mechanisms of GHGs in the occluded gas within the ice wedge were constrained by analyzing carbon stable isotopes of the GHGs (CO₂, CH₄) and the sediment particles included in the wedge ice, the relationships between the mixing ratios of GHGs (CO₂, N₂O, CH₄), and various soluble inorganic ionic compositions of the wedge ice. The Ar/N₂/O₂ compositions indicated that the studied ice wedges were likely formed through dry snow or hoarfrost compaction, and microbial activity remained active after ice wedge formation. The $\delta^{18}\text{O}$ and δD values of the ice suggested colder winter temperatures in the UIC compared to the LIC. CO₂ and CH₄ primarily originated from biogenic sources. N₂O showed exclusive correlation with CH₄, and its mixing ratios vary at different depths, likely due to differences in the microbiome. These findings suggest that GHG formation in ice wedges is not solely controlled by physiochemical conditions but involves a complex interplay between microbial activity and environmental conditions. Our study contributes to a better understanding of the dynamics involved in GHG formation within permafrost.

Keyword : Batagay megaslump, Greenhouse gases, Ice wedge, Water stable isotopes, Permafrost, Northeastern Siberia

Student Number : 2021-29005

Table of Contents

Chapter 1. Introduction	1
Chapter 2. Site and sample description.....	5
Chapter 3. Materials and Methods.....	7
3.1 Gas extraction and mixing ratio measurements.....	7
3.2 Stable water isotope analysis.....	9
3.3 Soil and major ion chemistry.....	10
3.4 Stable carbon isotopes for greenhouse gas	11
Chapter 4. Results.....	12
4.1 Stable water isotopes	12
4.2 N ₂ , O ₂ and Ar mixing ratios	13
4.3 Greenhouse gas mixing ratios	14
4.4 Soil and ion properties.....	15
4.5 δ ¹³ C for greenhouse gas	16
Chapter 5. Discussion	17
5.1 Batagay ice wedge formation and related climate conditions.....	17
5.2 Origin of GHGs within ice wedges.....	20
5.2.1 Carbon dioxide, CO ₂	23
5.2.2 Methane, CH ₄	24
5.2.3 Nitrous oxide, NO ₂	26
Chapter 6. Conclusion	31
References	32
Abstract in Korean.....	38
List of Figures.....	39
List of Tables	47

Chapter 1. Introduction

In the current global warming crisis, the rapid increase in greenhouse gas (GHG) in the atmosphere is of great concern. It is crucial to identify the processes involved in GHG formation and estimate its potential for emissions into the atmosphere. Because GHG species are associated significantly with the global carbon and nitrogen cycles, one must acknowledge active or inactive carbon and nitrogen reservoirs as well as their chemical reactions. Permafrost contains a large reservoir of organic carbon and nitrogen in terrestrial regions and it is an active area of research on active global carbon and nitrogen cycles.(Hugelius et al. 2014; Salmon et al. 2018) Multiple evidences show that permafrost may emit a significant amount of GHGs into the atmosphere via thawing, thus accelerating global warming.(Liljedahl et al. 2016) Yedoma, which is an Late Quaternary organic and ice-rich permafrost deposit around East Siberia and Alaska, has a higher ice content than typical permafrost soils and is highly susceptible to climate change. The Intergovernmental Panel on Climate Change (IPCC) reported that permafrost regions are more sensitive to global warming owing to their high latitudinal location; hence, GHG formation from the Yedoma deposits is a key factor affecting further GHG emissions.(Pörtner, Roberts, and Masson-Delmotte 2022)

Although permafrost can be distinguished based on several features, ice wedges are characteristic of permafrost regions. Ice wedges are formed when thermal contraction cracks appear in the ground during winter.(Opel et al. 2018) The cracks are filled via two main processes: meltwater refreezing and snow/hoarfrost accretion infilling.(St-Jean et al. 2011) Additionally, sediment and soils on the land

surface or active layers can enter frost cracks with water or snow and define foliation in ice wedges. Soils combined with water and snow may facilitate microbial activities related to GHG formation. Although GHG emissions from permafrost soils have been investigated comprehensively,(Brouchkov and Fukuda 2002; Teepe, Brumme, and Beese 2001; Öquist et al. 2004) previous studies pertaining to ice wedges are primarily limited to winter climate reconstructions and stable water isotope analysis.(Wetterich et al. 2021) Meanwhile, studies that directly measure the mixing ratios of GHGs and the compositions of other gases within ground ice and ice wedges are few.(Kyungmin Kim et al. 2019; Boereboom et al. 2013; J. Yang et al. 2022)

Investigations pertaining to ice wedges in Alaska and Siberia, particularly in Yakutia, have progressed, with emphasis on the analysis of ice wedges in lowland areas near rivers or coastlines. However, ice wedges in continental highlands are rarely investigated. The Batagay megaslump is located in the Yana Highlands, which are characterized by highly continental climate conditions north of the Arctic Circle. The nearby settlement Verkhoyansk is known as the cold pole of the Northern Hemisphere.(Ashastina et al. 2017) Therefore, the Yana Uplands are considered to have the most extreme continental climate in the Northern Hemisphere. The exposure of the Batagay megaslump provides valuable data pertaining to GHGs within the ice wedges formed under continental conditions. This megaslump has experienced rapid thawing and significant growth in the past, with a thermo-denudation rate of 15 m/year. As of 2019, the maximum width of the slump was 890 m.(J. Murton et al. 2023)

Because of its exposed stratigraphy and active thawing of permafrost, the Batagay megaslump reveals the presence of ice wedges that formed during the

Middle and Late Pleistocene.(J. B. Murton et al. 2022) This exposure allows one to obtain paleo-environmental and biogeochemical information for these times.(Jongejans et al. 2022) The absence of peatland soils indicates that this area did not undergo a thermokarst process.(Ashastina et al. 2017) The ancient syngenetic permafrost exposed in the Batagay megaslump suggests that gas bubbles and sediments trapped within the ice wedges may have preserved valuable information pertaining to the environmental conditions at the time of their formation. Additionally, ice wedges serve as a sanctuary for diverse and active microbial communities in cold permafrost regions, and the presence of active microorganisms contributes to the formation of GHGs.(Wilhelm et al. 2012)

The formation and emission potentials of GHGs differ across different regions as well as different layers and depths in a region. These spatial differences may be due to the biogeochemical and environmental factors in each region. I compared two different stratigraphic units of the Batagay megaslump. They might reflect different paleoenvironmental factors, thus suggesting that they affect carbon/nitrogen pools and microbiomes differently during GHG formation. The potential of GHG formation and emission potentials from permafrost of the Batagay megaslump is obvious from the high wedge ice content in both ice oversaturated Ice Complex deposits; amounting up to 70 vol% in the UIC and 56 vol% in the LIC.(Kizyakov et al. 2023)

In this study, I analyzed the gas in bubbles entrapped in ice wedges from two ice complex units of the Batagay megaslump. The soil and stable water isotope chemistries are analyzed as well. The objectives of this study are (1) to propose a possible formation process for Batagay ice wedges based on air composition (Ar/N₂/O₂) and stable water isotopes to predict the occurring gas-forming reactions

in a stable system and under climatic conditions during formation, and (2) to propose possible biogeochemical processes of GHG formation for both ice complex units under subfreezing temperatures.

Chapter 2. Site and sample description

Ice wedge samples were obtained from the Batagay megaslump region (67.58°N, 134.77°E) in north-eastern Siberia, Russia (Figure 1). The Batagay megaslump is near the village of Batagay on the east bank of the Yana River in the Yana Highlands. It is situated on a hillslope at an elevation of approximately 290 m above sea level and is known as the world's largest thaw slump.(Ashastina et al. 2017; Opel et al. 2019; J. Murton et al. 2023) The region is characterized by a strong continental climate and increasing temperature and precipitation since the mid-twentieth century.(J. Murton et al. 2023) The permafrost is continuous and 200–500 m thick, whereas the active layer is 0.2–1.2 m thick. The vegetation near Batagay mainly comprises open woodlands dominated by Dahurian larch (*Larix dahurica*) with birch undergrowth and lichen-green moss ground cover.

The Batagay megaslump exposes Pleistocene and Holocene permafrost formations spanning from at least Marine Isotope Stage (MIS) 16 to 1.(J. B. Murton et al. 2022) Previous studies have identified six main stratigraphic units in the area.(Ashastina et al. 2017; Opel et al. 2019; J. B. Murton et al. 2022; 2017) The lowest unit comprises clasts-supported diamicton. The LIC (MIS 16) above includes V-shaped ice wedges that are 2–3 m high and approximately 1 m wide at the top, and are truncated by thaw unconformities. The lower sand unit (~MIS 7 to 4) is approximately 20 m thick and composed of yellowish pore ice-cemented sand with gray horizontal bands. It contains narrow syngenetic ice wedges up to 0.5 m wide. The UIC (MIS 4 to 3), which is 20–25 m thick, is dominated by large syngenetic ice wedges.(Opel et al. 2019)

For my study, I examined samples from three ice wedges from the LIC and 10

samples from four ice wedges of the UIC (Figure 2). In the LIC, the ice wedge samples were labeled as B19-IW1-gas, B19-IW3-gas, B19-IW5-gas, while in the case of UIC, as B19-IW8-gas1, 2; B19-IW9-gas1, 2, 3, 4; B19-IW10-gas1, 2; and B19-IW11-gas1, 2. The samples were cut from the ice wedges with a chain saw as huge blocks(approximate size 25x15x15 cm).

Chapter 3. Materials and Methods

3.1 Gas extraction and mixing ratio measurements

Dry and wet (melt–refreeze) extraction methods were used to extract the gas enclosed in the ice wedge samples. Both methods have the same purpose; however, wet extraction is predominantly used owing to its high air yield. Both extraction systems were employed at the SNU.(Kyungmin Kim et al. 2019; Ryu, Ahn, and Yang 2018) The details of the extraction systems have been compared comprehensively by Yang et al.(J. W. Yang et al. 2020) I extracted 22 subsamples via dry extraction and 33 subsamples via wet extraction. Most of the ice wedge subsamples were cut using a band saw. However, in situations where the band saw proved insufficient for cutting through high-hardness ice, a hand saw and a hammer were employed as alternatives. For gas extraction, 33 g of ice was used in the dry extraction method. As the dry extraction system can only measure a maximum of 12 g of ice simultaneously, I conducted three separate attempts to obtain data for one subsample. For the wet extraction, I placed 50 g of ice in a glass bottle. The gas extracted from the ice wedges was trapped at -256°C using a He closed-cycle refrigerator, which effectively cryogenically preserved the gas in a stainless-steel tube. To remove water vapor, I used a cold trap with ethanol at -85°C in dry extraction and soaked the glass bottles in an ethanol bath at -70°C for approximately 20 minutes in wet extraction. After trapping, the sample tubes were sealed, heated to room temperature, and separated into 2 tubes for measure air composition ($\text{Ar}/\text{O}_2/\text{N}_2$) and greenhouse gas mixing ratios (CO_2 , CH_4 , NO_2). After wet extraction, I preserved the remaining water and soil mixtures in high density polyethylene (HDPE) bottles and stored them in a freezer at -20°C for later use.

The gas mixing ratios were measured simultaneously using three gas chromatography (GC) systems. An Agilent 7890A GC system equipped with a flame ionization detector (FID) and a catalyst methanizer was employed to measure CO₂ mixing ratios. The N₂O and CH₄ concentrations were measured using an Agilent 7890B GC system equipped with an electron capture detector and FID. To measure the mixing ratios of Ar, O₂, and N₂, a 7890A GC system equipped with a FID/TCD was utilized. The values of Ar, O₂, and N₂ were used as indicators of gas alteration during or after ice wedges were formed. The $\delta(N_2/Ar)$ and $\delta(O_2/Ar)$ values were expressed as percentages (%) of the present-day molar atmospheric ratio using the following equation, where X represents N₂ or O₂:

$$\delta \left(\frac{X}{Ar} \right) = \left(\frac{\left(\frac{X}{Ar} \right)_{sample}}{\left(\frac{X}{Ar} \right)_{air}} - 1 \right) \times 100 \text{ (\%)}$$

During the Quaternary, the atmospheric molar ratios of N₂/Ar and O₂/Ar remained almost constant.(HOLLAND 1984) Consequently, the changes in these values can serve as indicators of gas alteration during or after ice wedge formation.

3.2 Stable water isotope analysis

Stable water isotope composition analysis ($\delta^{18}\text{O}$ and δD) for the ice wedges was conducted using meltwater that remained after the wet extraction process. The meltwater samples were centrifuged and filtered to remove organic matter and microparticles using a 0.45 μm syringe filter. The filtered samples were placed inside PVC bottles and stored in a freezer at -20°C until stable isotope analysis was performed. The stable water isotopic compositions were analyzed at Ewha Womans University, Korea, using an L2140-i model isotopic water liquid analyzer (Picarro Inc., Sunnyvale, CA, USA) based on the wavelength-scanned cavity ring-down spectroscopy method. The standards were Vienna Standard Mean Ocean Water 2 (VSMOW2), Standard Light Antarctic Precipitation (SLAP), USGS 46, 47, and 48, whose mean standard deviations were less than 0.9 ‰ for $\delta^{18}\text{O}_{\text{ice}}$ and less than 0.8 ‰ for δD . A total of 11 and 29 samples were obtained from the LIC and UIC, respectively. The isotopic ratios were expressed in per mill (‰) relative to the standard mean ocean water (SMOW) using the following equation: $R = {}^{18}\text{O}/{}^{16}\text{O}$ or D/H .

$$\delta_{\text{Sample}} = \left(\frac{R_{\text{Sample}}}{R_{\text{Standard}}} - 1 \right) \times 1000 \text{ (‰)}$$

3.3 Soil and major ion chemistry

To analyze the soil and major ion chemistry, I obtained 3 mL of filtered water and stored it in HDPE bottles. Both anions (Cl^- , NO_3^- , NO_2^- , SO_4^{2-}) and cations (NH_4^+ , Ca^{2+} , Mg^{2+} , Na^+ , K^+) were analyzed using an ion chromatograph at the National Instrumentation Center for Environmental Management (NICEM, Seoul National University, Seoul, Republic of Korea). For total Fe concentration, I analyzed 10mL of filtered water using an Inductively Coupled Plasma-Mass Spectrometry (ICP-MS) at the NICEM.

I separated the soil samples and dried them under ambient conditions for 48 h. After the soils were completely dried, I used Midwood and Boutton's (1998) method to remove carbonate minerals.(Midwood and Boutton 1998) For the removal, I performed the following steps: 0.3 g soil for each sample was soaked in 0.5 M HCl solution. The soil-HCl solution was maintained at 24 h and stirred thrice during the reaction. Subsequently, they were separated via centrifugation at 4000 RPM for 7 min. Next, they were washed with deionized water four times via the same centrifugation process. Meanwhile, the soils were dried at 87 °C for 24 h, stored in a 1.5 mL conical tube, and sent to NICEM for the analyses of $\delta^{13}\text{C}$, $\delta^{15}\text{N}$, total carbon, and total nitrogen.

3.4 Stable carbon isotopes for greenhouse gas

I determined the carbon isotope ratios of CO₂ and CH₄ to identify their sources. The wet extraction method was used to extract CO₂ and CH₄, which were then stored in stainless-steel tubes for subsequent analysis. The $\delta^{13}\text{C-CO}_2$ and $\delta^{13}\text{C-CH}_4$ values were measured at Nagoya University, Japan, using a CF-IRMS system. (Tsunogai et al. 2000; Kawagucci et al. 2005; Hirota et al. 2010) Three samples from both the LIC and UIC were analyzed for $\delta^{13}\text{C-CO}_2$, whereas one sample from the LIC and two samples from the UIC were measured for $\delta^{13}\text{C-CH}_4$. The mean standard deviation was 0.1‰–0.2‰ for $\delta^{13}\text{C-CO}_2$ and < 0.2‰ for $\delta^{13}\text{C-CH}_4$.

Chapter 4. Results

4.1 Stable water isotopes

The $\delta^{18}\text{O}$ and δD values of the LIC ranged from -32.82‰ to -30.58‰ and -251.04‰ to -234.65‰ respectively. The UIC showed more depleted values of $\delta^{18}\text{O}$ and δD than the LIC, which ranged from -33.05‰ to -36.63‰ and -259.30‰ to -284.74‰, respectively (Table 1, Figure 4). The deuterium excess (d-excess) values of the LIC and UIC were 7.72‰ to 18.14‰ and 4.64‰ to 10.96‰, respectively. The linear regression between $\delta^{18}\text{O}$ and δD yielded equations of $\delta\text{D} = 7.3189 \times \delta^{18}\text{O} - 15.746$ and $\delta\text{D} = 9.3108 \times \delta^{18}\text{O} + 54.243$ for the LIC and UIC, respectively. Comparing our results with those of Opel et al., (Opel et al. 2019) the UIC samples were within the same range and followed the global meteoric water line (GMWL). However, compared with Opel et al., (Opel et al. 2019) the LIC samples showed enriched $\delta^{18}\text{O}$ and δD , a much wider range of stable isotope values, and a steeper slope as compared with the GMWL.

4.2 N₂, O₂ and Ar mixing ratios

The $\delta(\text{N}_2/\text{Ar})$ molar ratios or other noble gas ratios can be analyzed to elucidate the formation process of ice wedges. N₂ and other noble gases are not significantly affected by biological activity and exhibit different solubilities in water. If ice wedges have undergone physical processes, such as melt–refreezing or formation from liquid water, then the $\delta(\text{N}_2/\text{Ar})$ value is likely to be below 0 and potentially close to -55.5%. This is based on the assumption that atmospheric gases equilibrate with water at the freezing point and that the gas composition remains unchanged during freezing. By contrast, if ice is formed through snow compaction or have not undergone melt–refreezing, then the $\delta(\text{N}_2/\text{Ar})$ value should be approximately 0%. (St-Jean et al. 2011) Our measurements of $\delta(\text{N}_2/\text{Ar})$ in the Batagay ice wedges ranged from -8.06% to 33.86% for the LIC and from 5.49% to 30.64% for the UIC. These values suggest a minimal melting effect or its absence on the Batagay ice wedges (Figure 5).

The $\delta(\text{O}_2/\text{Ar})$ ratio serves as an indicator of biological activity. In the absence of biological activities in the ice wedges, we can expect $\delta(\text{O}_2/\text{Ar})$ to be approximately 0%. However, a $\delta(\text{O}_2/\text{Ar})$ value of below 0 suggests the presence of biological activities, as most underground biological processes consume oxygen gas. The $\delta(\text{O}_2/\text{Ar})$ values ranged from -89.01% to -67.43% and -98.07% to -47.06% for the LIC and UIC, respectively. These values indicate the presence of biological activity in the ice wedges.

4.3 Greenhouse gas mixing ratios

The mean CO₂, CH₄, and N₂O mixing ratios (1σ) of the Batagay ice wedge for the LIC and UIC were 3.88 ± 2.14%, 3.90 ± 2.23% %, 90.08 ± 47.51 ppm , 54.97 ± 24.94 ppm, and 1.16 ± 2.05 ppm, 19.45 ± 25.30 ppm, respectively (Table 1, Figure 6). These GHG mixing ratios in gas bubbles in the Batagay ice wedges were two to three orders of magnitude greater than those at the Pleistocene atmospheric level.(Lüthi et al. 2008; Loulergue et al. 2008; Schilt et al. 2010) The relationship between the GHG mixing ratios in the Batagay ice wedges did not indicate any significant correlations, except for the exclusive relations between the N₂O and CH₄ mixing ratios (Figure 7). When compared with ice wedges in other Siberian regions, specifically those located in the interior of Yakutia, such as Churapcha, Cyuie, and Syrdakh, the Batagay ice wedges generally exhibited low CO₂ but high N₂O and CH₄ levels (Figure 8).(J. Yang et al. 2022; Kyungmin Kim et al. 2019)

4.4 Soil and ion properties

The mean soil contents (1σ) of the LIC and UIC ice wedge samples were 0.0136 ± 0.0038 and 0.0179 ± 0.0158 g/g_{ice}, respectively (where g_{ice} is the unit weight of an ice and soil mixture from an ice wedge). The mean carbon and nitrogen ratios, C/N (1σ) for the LIC and UIC were 9.76 ± 1.18 and 10.19 ± 0.84 , respectively; their mean $\delta^{13}\text{C}$ values (1σ) were -25.80 ± 0.09 ‰ and -25.56 ± 0.24 ‰; and their mean soil $\delta^{15}\text{N}$ values (1σ) were 3.38 ± 2.23 ‰ and 4.10 ± 0.24 ‰, respectively (Table 1). In general, both the LIC and UIC exhibited similar soil characteristics, and their chemical activities might be similar regardless of the formation age.

Ion and Fe concentrations in the meltwater samples from LIC and UIC are described in Table 3. In particular, NO_3^- concentrations were 9.21 mg/L (n=1) and 10.13 ± 0.15 mg/L (n=2) for the LIC and UIC, respectively. NH_4^+ concentrations were 2.25 ± 1.42 mg/L (n=5) and 2.13 ± 1.08 mg/L (n=4) mg/L for the LIC and UIC, respectively. It should be noted that NO_2^- concentrations were only measured in the UIC samples, and the concentration was 1.58 ± 1.44 mg/L (n=3). The LIC samples either were not measured or fell below the detection limit for NO_2^- . Additionally, the Fe concentrations were 386.11 ± 216.84 $\mu\text{g/L}$ (n=5) and 47.50 ± 67.82 $\mu\text{g/L}$ (n=5) for the LIC and UIC, respectively.

4.5 $\delta^{13}\text{C}$ for greenhouse gas

The $\delta^{13}\text{C}$ values for CO_2 were $-22.8 \pm 1.80\text{‰}$ (n=3) and $-23.8 \pm 1.43\text{‰}$ (n=3) for the LIC and UIC, respectively, whereas those for CH_4 were $-48.1 \pm 1.12\text{‰}$ (n=2) and -36.7‰ (n=1), respectively.

Chapter 5. Discussion

5.1 Batagay ice wedge formation and related climate conditions

I used the gas composition and water-stable isotopes to assess ice wedge formation and the related climatic conditions. Our $\delta(N_2/Ar)$ values relative to atmospheric air were approximately 0% or greater (Figure 5). This suggests that the ice wedges were not formed by freezing of liquid snowmelt water, but rather by the compaction of dry snow or hoarfrost. The shapes of the bubbles within the ice wedges also provide information regarding their formation. If ice wedges formed by refreezing of meltwater, then the bubbles generated may exhibit elongated shapes and a preferred orientation. However, upon examining thin sections (~2 mm thick) of the Batagay ice wedges, we observed spherical bubbles in the both ice complexes (Figure 3). Meanwhile, upon inspecting the bulk ice blocks, we did not observe any perturbations in the foliation, thus indicating that the ice wedges were not disrupted by melting after formation.

The $\delta(N_2/Ar)$ values ranging from 10% to 20% in the Batagay ice wedges, are greater than the typically observed values of approximately or less than 0% in other Siberian ice wedges (Figure 5). To explain this elevation in the N_2/Ar values, we may consider a differential gas diffusion through the ice lattice by faster Ar diffusion than N_2 through ice. Previous studies have confirmed that gas molecules can diffuse through ice via interstitial or bond-breaking mechanisms, as supported by molecular dynamics (MD) simulations.(Ikeda-Fukazawa, Kawamura, and Hondoh 2004; Ikeda-Fukazawa et al. 2002; 2005; Yi et al. 2021) To quantify this effect, I employed equations for gas permeation coefficients (diffusion coefficients

× solubility) in ice. Using the parameters described by Oyabu et al. (Oyabu et al. 2021), I calculated the permeation coefficients for N₂ and Ar at -10°C, and obtained 1.31×10^{-19} and $4.16 \times 10^{-19} \text{ m}^2/\text{s} \cdot \text{MPa}$, respectively. These values indicate that the permeability of Ar is higher than that of N₂. Consequently, the N₂/Ar ratio in the Batagay ice complex units can be increased by gas diffusion in ice matrix. I observe that the LIC generally exhibited greater N₂/Ar values than the UIC. This difference may be caused by that the LIC was located at a greater depth, experiencing higher pressures and having longer time (~ 650 ka for LIC vs. ~ 40 ka for UIC) for the differential diffusion than the UIC.

Stable water isotope ratios of ice wedge ice can be used to investigate winter temperature conditions during the ice wedge formation, with a positive correlation between the winter temperatures and δ¹⁸O values. (Yurij K. Vasil'chuk et al. 2020) I observed that the UIC exhibited depleted δ¹⁸O values as compared to the LIC, with a difference of approximately 2.7‰ (Figure 4, Table 1). This suggests that the LIC was formed at relatively higher winter temperatures (2.7°C) (Yu K. Vasil'chuk 1991) as compared with the UIC. These differences might due to from glacial-interglacial climatic conditions in the UIC and the LIC. (Courtin et al. 2022)

The potential effect of isotopic fractionation on the use of ice wedges as archives for winter temperature must be considered as it can alter the original isotopic signature of ice. (Meyer et al. 2002; Opel et al. 2011) Sublimation can enrich heavier isotopes in the ice, thus resulting in a lower slope than that of the GMWL. In the Batagay ice wedge samples, the isotopic compositions of δD and δ¹⁸O aligned with the GMWL and the local meteoric water line of Yakutsk. Furthermore, the δ¹⁸O values of the ice wedges generally reflected a similar trend to that reported by Opel et al. (Opel et al. 2019) These observations suggest that the isotopic

compositions are unlikely to be caused by sublimation process.

5.2 Origin of GHGs within ice wedges.

To understand the origin of GHGs entrapped in ice wedges, one must verify whether the ice wedges have been maintained in a stable state without being subjected to processes such as breakage or disruption. The Batagay megaslump ice wedges appeared to be unaltered and well-preserved under stable conditions, as indicated by the undisrupted foliation and spherical bubble shapes as well as the zero to positive values of $\delta(\text{N}_2/\text{Ar})$ relative to the atmospheric N_2/Ar ratio. Hence, we can assume that the ice wedges from the Batagay permafrost are quasi-closed and stable systems. Meanwhile, as Batagay ice wedges are likely formed by snow and/or hoarfrost compaction, it is likely that the initial mixing ratios of GHGs are atmospheric values, and that the observed high mixing ratios of GHG in the bubbles of the Batagay ice wedges are due to the formation of GHG inside the ice wedges.

The dissolution of atmospheric GHG (CO_2 , CH_4 and N_2O) in liquid water can increase the mixing ratios of GHGs. If an equilibrium exists between air and snow/ice meltwater, then the GHG mixing ratios in the liquid water can increase up to 60, 2, and 45 times the atmospheric level for CO_2 , CH_4 and N_2O , respectively.(J.-W. Yang et al. 2017) Consequently, if the snowmelt-refreeze process is involved in ice wedge formation, then we can expect the GHG mixing ratios in ice wedges to be up to 16800, 1.4 and 12.6 ppm for CO_2 , CH_4 and N_2O , respectively.(Kyungmin Kim et al. 2019) However, because evidence of melting during or after ice wedge formation was not indicated, I precluded this process as the main source of GHGs in ice wedges.

Microbial activity has been shown to persist even at soil temperatures below

0°C.(Nikrad, Kerkhof, and Häggblom 2016; Katayama et al. 2007) Despite having limited substrates and energy sources for their metabolic processes, these microorganisms are crucial in maintaining high mixing ratios of GHGs in ice wedges. Bacteria can remain viable for thousands of years through active reproduction or by maintaining the minimal activity levels necessary for the repair of cellular damage. In permafrost, the necessary energy for sustaining cellular functions or facilitating reproduction can be potentially derived from nutrients released from frozen sediments.(Bakermans et al. 2003) In Batagay ice wedges, the main source of nutrients might be the soils entrapped during the ice wedge formation.

The initial air composition(O₂, N₂, Ar) during the formation of ice wedges would have been similar to that of the atmosphere.(St-Jean et al. 2011) However, microbial activity in the ice wedge that consumes oxygen may result in aerobic to anaerobic or oxygen-depleted conditions. Notably, the heterogeneous distribution of the soil content in ice wedges must be considered, as the presence or absence of oxygen can vary across different microsites in an ice wedge. Furthermore, the permeability of gas molecules can influence the mixing ratios in ice bubbles. O₂ and Ar have higher permeation coefficient (4.16×10^{-19} and $3.39 \times 10^{-19} \text{ m}^2/\text{s} \cdot \text{MPa}$, respectively) than N₂ ($1.31 \times 10^{-19} \text{ m}^2/\text{s} \cdot \text{MPa}$) and major greenhouse gases (CO₂, : 1.39×10^{-19} and CH₄ : $7.08 \times 10^{-20} \text{ m}^2/\text{s} \cdot \text{MPa}$, N₂O is not constrained) at -10°C.(Ahn et al. 2008; Kyungmin Kim et al. 2019) Consequently, due to these differences in permeability, the mixing ratios of O₂ and Ar are likely to decrease, while the mixing ratios of N₂, CO₂ and CH₄ may increase in ice bubbles. However, the increase of CO₂ mixing

ratio by the gas diffusion is not likely more than that of N₂ due to the similar permeation coefficients (1.39 vs. $1.31 \times 10^{-19} \text{ m}^2/\text{s} \cdot \text{MPa}$).

5.2.1. Carbon dioxide, CO₂

The observed high CO₂ mixing ratios in the ice wedges may be caused by biological respiration, which is a process that consumes O₂ and produces CO₂. The stable carbon isotope ratio of CO₂ can provide valuable information regarding the source of CO₂ entrapped in ice wedges. (Lachniet, Lawson, and Sloat 2012) The average $\delta^{13}\text{C}$ -CO₂ values for the LIC and UIC samples were determined to be $-22.8 \pm 1.80\text{‰}$ (n = 3), $-23.8 \pm 1.43\text{‰}$ (n = 3), respectively. These values are within the range of carbon isotope values of CO₂ derived from soil organic carbon ($\delta^{13}\text{C} = -25.8 \pm 0.09 \text{‰}$, n = 5 for LIC; $\delta^{13}\text{C} = -25.56 \pm 0.24 \text{‰}$, n = 5 for UIC), but very different from those of preindustrial atmospheric CO₂ ($\delta^{13}\text{C} = -6.7\text{‰}$). (Rubino et al. 2013) Thus, the isotopic ratios indicate that the CO₂ in Batagay ice wedges were mostly originated from microbial oxidation of soil organics although the mean values of $\delta^{13}\text{C}$ -CO₂ were slightly greater than the soils in the Batagay ice wedges. Mixing with atmospheric CO₂ could increase the $\delta^{13}\text{C}$ -CO₂ values. However, the observed CO₂ mixing ratios were approximately 160 times greater than the atmospheric values from LGM. (Hönisch et al. 2009) Meanwhile, the weathering of carbonate minerals, which typically indicate a $\delta^{13}\text{C}$ value of approximately 0‰, can increase carbon isotope values. (Land 1980) Based on mass balance calculation, I estimated that the CO₂ production from the carbonate minerals can explain less than 12 % of the CO₂ in the bubbles. Hence, I concluded that most of the CO₂ in Batagay ice wedges originated from biological respiration.

5.2.2 Methane, CH₄

There are both abiotic and biotic CH₄ production processes.(Etiopie and Sherwood Lollar 2013) Most abiotic processes require suitable thermal conditions (300 °C–400 °C) instead of subfreezing conditions.(Etiopie and Sherwood Lollar 2013) Despite the recent exposure of the Batagay megaslump due anthropogenic disturbance, the permafrost and ice wedges in the area remain in a stable state, characterized by low temperatures. Furthermore, the undisturbed foliations observed in the ice wedges indicate that they were not affected by geothermal and physical activity during or after their formation. Hence, I can exclude the thermogenic process as the primary source of CH₄ in the Batagay ice wedges.

The carbon isotope ratios of methane can provide valuable information about methane production processes in permafrost regions.(Whiticar 1999; Rivkina et al. 2007; Høj, Olsen, and Torsvik 2005) Courtin et al.,(Courtin et al. 2022) identified certain methanogenic archaea in the Batagay ice complex units (UIC, LIC), indicating the possibility of biogenic processes occurring in ice wedges. According to Whiticar et al.,(Whiticar 1999) the $\delta^{13}\text{C-CH}_4$ value of the LIC (-47.3‰, -48.9‰) is indicative of bacterial origin (< -45‰), whereas the $\delta^{13}\text{C}$ value of the UIC (-36.7‰) indicates thermogenic origin (-20‰ to -50‰). However, since we have already excluded the possibility of thermogenic CH₄ production, the relatively enriched $\delta^{13}\text{C-CH}_4$ value from the UIC could be attributable to isotopic fractionation during its exchange with and transformation to CO₂. Whiticar et al.,(Whiticar 1999) suggested using the isotopic separation factor (ϵ_c), where $\epsilon_c = \delta^{13}\text{C-CO}_2 - \delta^{13}\text{C-CH}_4$, to infer the methane production or consumption process. In this study, the LIC and UIC exhibited ϵ_c values of 24.5 and 12.9, respectively,

which were within the range for methane oxidation. Furthermore, methane-oxidizing bacteria have been reported to alter the carbon isotope composition of CH₄.(Barker and Fritz 1981) These bacteria preferentially consume ¹²C, thus yielding values of lighter isotopes in the resulting CO₂, whereas the remaining CH₄ becomes enriched in heavier isotopes. This can potentially result in the misinterpretation of biogenic CH₄ signatures as natural gas deposits or having thermogenic origins. Earlier studies have shown a correlation between anaerobic methane oxidation and reductions in nitrate and sulfate, suggesting that methane oxidation can occur even in anaerobic conditions.(McGlynn et al. 2015; Haroon et al. 2013) Therefore, it is plausible that methane in ice wedges may have undergone such processes, potentially impacting its isotopic composition.

5.2.3 Nitrous oxide, N₂O

Compared with atmospheric levels in the Middle Pleistocene and Holocene (200–300 ppb),(Schilt et al. 2010) the elevated N₂O mixing ratios in the Batagay ice wedges may be attributed to N₂O production in the ice wedges.

Microbial nitrification and denitrification processes were considered for the N₂O production pathways in permafrost-affected soils.(Voigt et al. 2020) In the case of Batagay, both nitrification and denitrification process can be potential sources of N₂O due to the heterogeneous distribution of oxygen gas in the Batagay ice wedges.(Tiedje 1988) Multiple studies have demonstrated that N₂O production can remain active in seasonally frozen soils, even at subzero temperatures, thus indicating that the soils within ice wedges can produce N₂O within the ice wedge system.(Öquist et al. 2004; Voigt et al. 2020) Nitrification is a strictly aerobic condition that requires O₂ as an electron acceptor for a series of oxidative reactions that convert NH₄⁺ to NO₂⁻ and NO₃⁻. This process is facilitated by ammonia-oxidizing archaea and bacteria, which produce N₂O as a byproduct. The low O₂ mixing ratios in the ice complexes from Batagay (< 5%) suggest that nitrification dominates in the initial stages of ice wedge formation but may not be the dominant source of N₂O production in the later stage.(Tiedje 1988; Khalil, Mary, and Renault 2004) However, significant N₂O emissions through nitrification have been observed under low-oxygen conditions in other studies;(Bateman and Baggs 2005) therefore, we cannot completely preclude the significant contribution of nitrification in a later stage.

In denitrification, both NO₂⁻ and NO₃⁻ act as electron acceptors for denitrifiers in an anaerobic respiration pathway, thus resulting in their reduction to

N₂, with NO and N₂O as gas intermediates.(Zhu et al. 2013) Soil incubation studies demonstrated that N₂O can be produced by denitrification and nitrifier-denitrification under low oxygen condition.(Zhu et al. 2013; Nathaniel E. Ostrom et al. 2010) Under completely anoxic conditions, N₂O is predominantly produced through denitrification.(Zhu et al. 2013) Hence, it can be expected that denitrification and nitrifier-denitrification are dominant processes under low oxygen condition periods.

An exclusive relationship between the N₂O and CH₄ mixing ratios was observed in Batagay. In the LIC, low CH₄ was accompanied by very high N₂O mixing ratios, and vice versa for the UIC (Figure 7b). This pattern is consistent with previous findings pertaining to other ice wedges from Siberia, where the distribution of CH₄ and N₂O mixing ratios showed distinct characteristics (Figure 8b).(Kyungmin Kim et al. 2019; J. Yang et al. 2022) This exclusive relationship may be explained by the inhibitory effect of N-containing compounds (NO₃⁻, NO₂⁻, NO, and N₂O) on methanogenesis. Several studies have reported a decrease in methanogenic bacterial activity in the presence of N₂O.(Klüber and Conrad 1998; J. Yang et al. 2022) Hence, the low N₂O mixing ratios and relatively high CH₄ mixing ratios in the LIC is attributable to its low potential to generate N-containing compounds, including N₂O, which subsequently promotes more active methanogenesis.

Meanwhile, the average N₂O mixing ratios in the UIC were considerably higher than those in the LIC. In order to elucidate this phenomenon, I examined two perspectives related to vegetation and microorganisms. Vegetation can affect environmental factors, such as soil pH and nutrient cycling. Therefore, the differences in vegetation between the UIC and LIC can provide insights into the

variation in biogeochemical factors for N₂O production. Courtin et al. suggest that LIC reflects interglacial ecosystem which has open forests with grassland, and UIC reflects glacial ecosystem that herb communities dominated the vegetation. Although reference show that there are environmental differences between the UIC and LIC, our analysis of soil characteristics, including soil C/N ratios and $\delta^{13}\text{C}_{\text{PDB}}$ values (Table 1), in both ice complex units exhibit no significant differences. On the other hand, microbial activities and specific enzymes can play a crucial role in N₂O the processes of N₂O production. Previous studies showed the existence of different prokaryotic communities in the sediments of upper and lower units of the Batagay megaslump, with higher numbers of ammonia-oxidizing archaea (AOA) in the UIC than in the LIC sediments.(Courtin et al. 2022) Furthermore, numerous *Nitrososphaeraceae* and *Nitrosopumilaceae* families were detected, which constitute AOA families and are known to be key contributors to N₂O emissions in Arctic soils.(Prosser et al. 2020; Alves et al. 2019) These differences in the archaeal community may explain the variations in N₂O levels between the UIC and LIC. On the other hand, the different ages of the LIC and the UIC can influence N₂O mixing ratios. If denitrification activity is the same in both layers, the LIC would reduce more N₂O than the UIC due to having more reaction time. However, since the availability of NO₃⁻ is crucial in denitrification and AOA plays a significant role in creating NO₃⁻, the low abundance of AOA in the LIC reduces the likelihood of NO₃⁻ supply and further N₂O reduction. Hence, age differences might not significantly affect N₂O mixing ratios. Although a specific examination of the soil microbiome trapped inside the ice wedges was not conducted in this study, insights from the surrounding soils can provide some understanding regarding processes occurring in the ice wedges.

The abiotic processes involved in N₂O production in the ice wedges are chemo-denitrification (chemical reduction of NO₃⁻ by reaction with Fe²⁺) and the oxidation of NH₂OH,(Picardal 2012; Bremner, Blackmer, and Waring 1980) These processes are significantly influenced by ion availability. In my study, most of the ion (NH₄⁺, NO₃⁻, and NO₂⁻) concentration data were below the detection limit of 0.001 mg/L (Table 3). However, significantly small amount of (0.001mg/L) of ions have potential to create 10 to 20 ppm N₂O, we need to consider abiotic processes.

In some laboratory experiments, researchers have reported abiotic processes for N₂O production. These include chemo-denitrification, which involves the chemical reduction of NO₃⁻ through reaction with Fe²⁺, as well as the oxidation of NH₂OH in soils.(Bremner, Blackmer, and Waring 1980) However, such natural observations are relatively scarce. There was a notable instance of chemo-denitrification with Fe²⁺ reported in the brine of ice-sealed Vida Lake, Antarctica.(N. E. Ostrom et al. 2016) To investigate the possibility, we analyzed total Fe concentration and obtained values of 0.386 ± 0.216 mg/L and 0.048 ± 0.068 mg/L for the LIC and UIC, respectively (Table 3). These Fe concentrations are comparable to those found in the pore water and peat ice of the Western Siberian Lowland, which are 0.68 and 2.05 mg/L, respectively.(Lim et al. 2021) However, they are two orders of magnitude smaller than the reported Fe²⁺ concentration in the brine of Vida Lake, which was 17.195 ± 1.262 mg/L for Fe²⁺.(Murray et al. 2012; Lim et al. 2021) Further investigation is necessary to explore the possibility of these abiotic reactions, including the examination of proton concentrations (pH). Protons may have an impact on the abiotic reactions,(Gordon and Butler 1986) particularly within the ice veins and thin films around soil particles. These areas exhibit distinct geochemical conditions from bulk

environment, potentially due to freeze-concentration effects.(Kolhe, Amend, and Singh 2010; Kitae Kim et al. 2019; Le et al. 2020)

Chapter 6. Conclusion

The Batagay ice complex units have provided valuable biogeochemical information pertaining to ground ice in the Yana Uplands since the Middle Pleistocene. Our observations indicate that the ice wedges were formed by the compaction of dry snow and/or hoar frost, as indicated by the N_2/Ar ratios and bubble shapes. The higher mixing ratios of GHGs in the Batagay ice wedges compared with those in the Pleistocene atmosphere implied a substantial contribution from microbial activity in the ice wedges. The carbon stable isotope values suggested that CO_2 and CH_4 originated primarily from microbial sources. The high level of N_2O compared to the preindustrial atmosphere is attributable to microbial activity instead of abiotic factors. Notably, the UIC and the LIC units show differences in terms of N_2O mixing ratios, which is probably due to the UIC having more of specific ammonia-oxidizing archaeal families instead of environmental or climatic differences. This suggests that biogeochemical factors in ice wedges can vary even within the same location, thus highlighting that GHG formation in ice wedges is not solely controlled by physiochemical conditions. This study provides insights into the complex relationships between microbial activity and biogeochemical conditions for GHG formation and storage in permafrost ice wedges.

References

- Ahn, Jinho, Melissa Headly, Martin Wahlen, Edward J. Brook, Paul A. Mayewski, and Kendrick C. Taylor. 2008. "CO₂ Diffusion in Polar Ice: Observations from Naturally Formed CO₂ Spikes in the Siple Dome (Antarctica) Ice Core." *Journal of Glaciology* 54 (187): 685–95. <https://doi.org/10.3189/002214308786570764>.
- Alves, Ricardo J. Eloy, Melina Kerou, Anna Zappe, Romana Bittner, Sophie S. Abby, Heiko A. Schmidt, Kevin Pfeifer, and Christa Schleper. 2019. "Ammonia Oxidation by the Arctic Terrestrial Thaumarchaeote Candidatus Nitrosocosmicus Arcticus Is Stimulated by Increasing Temperatures." *Frontiers in Microbiology* 10 (JULY). <https://doi.org/10.3389/fmicb.2019.01571>.
- Ashastina, Kseniia, Lutz Schirrmeister, Margret Fuchs, and Frank Kienast. 2017. "Palaeoclimate Characteristics in Interior Siberia of MIS 6-2: First Insights from the Batagay Permafrost Mega-Thaw Slump in the Yana Highlands." *Climate of the Past* 13 (7): 795–818. <https://doi.org/10.5194/cp-13-795-2017>.
- Bakermans, Corlen, Alexandre I. Tsapin, Virginia Souza-Egipsy, David A. Gilichinsky, and Kenneth H. Nealson. 2003. "Reproduction and Metabolism at -10°C of Bacteria Isolated from Siberian Permafrost." *Environmental Microbiology* 5 (4): 321–26. <https://doi.org/10.1046/j.1462-2920.2003.00419.x>.
- Barker, James F., and Peter Fritz. 1981. "Carbon Isotope Fractionation during Microbial Methane Oxidation." *Nature* 293 (September): 289–91.
- Bateman, E. J., and E. M. Baggs. 2005. "Contributions of Nitrification and Denitrification to N₂O Emissions from Soils at Different Water-Filled Pore Space." *Biology and Fertility of Soils* 41 (6): 379–88. <https://doi.org/10.1007/s00374-005-0858-3>.
- Boereboom, T., D. Samyn, H. Meyer, and J.-L. Tison. 2013. "Stable Isotope and Gas Properties of Two Climatically Contrasting (Pleistocene and Holocene) Ice Wedges from Cape Mamontov Klyk, Laptev Sea, Northern Siberia." *The Cryosphere* 7 (1): 31–46. <https://doi.org/10.5194/tc-7-31-2013>.
- Bremner, J. M., A. M. Blackmer, and S. A. Waring. 1980. "Formation of Nitrous Oxide and Dinitrogen by Chemical Decomposition of Hydroxylamine in Soils." *Soil Biology and Biochemistry* 12 (3): 263–69. [https://doi.org/10.1016/0038-0717\(80\)90072-3](https://doi.org/10.1016/0038-0717(80)90072-3).
- Brouchkov, Anatoli, and Masami Fukuda. 2002. "Preliminary Measurements on Methane Content in Permafrost, Central Yakutia, and Some Experimental Data." *Permafrost and Periglacial Processes* 13 (3): 187–97. <https://doi.org/10.1002/ppp.422>.
- Courtin, Jérémy, Amedea Perfumo, Andrei A. Andreev, Thomas Opel, Kathleen R. Stoof-Leichsenring, Mary E. Edwards, Julian B. Murton, and Ulrike Herzschuh. 2022. "Pleistocene Glacial and Interglacial Ecosystems Inferred from Ancient DNA Analyses of Permafrost Sediments from Batagay Megaslump, East Siberia." *Environmental DNA*, no. May: 1–19. <https://doi.org/10.1002/edn3.336>.
- Etiopo, Giuseppe, and Barbara Sherwood Lollar. 2013. "Abiotic Methane on Earth." *Reviews of Geophysics* 51 (2): 276–99. <https://doi.org/10.1002/rog.20011>.
- Gordon, Louis I., and James H. Butler. 1986. "Rates of Nitrous Oxide Production in the Oxidation of Hydroxylamine by Iron(III)." *Inorganic Chemistry* 25 (25): 4573–77. <https://doi.org/10.1021/ic00245a024>.
- Haron, Mohamed F., Shihu Hu, Ying Shi, Michael Imelfort, Jurg Keller, Philip Hugenholtz, Zhiguo Yuan, and Gene W. Tyson. 2013. "Anaerobic Oxidation of Methane Coupled to Nitrate Reduction in a Novel Archaeal Lineage." *Nature* 500 (7464): 567–70. <https://doi.org/10.1038/nature12375>.
- Hirota, A., U. Tsunogai, D. D. Komatsu, and F. Nakagawa. 2010. "Simultaneous Determination of $\delta^{15}\text{N}$ and $\delta^{18}\text{O}$ of N₂O and $\delta^{13}\text{C}$ of CH₄ in Nanomolar Quantities from a Single Water Sample." *Rapid Communications in Mass Spectrometry* 24 (7): 1085–92. <https://doi.org/10.1002/rcm.4483>.
- Høj, Lone, Rolf A. Olsen, and Vigdis L. Torsvik. 2005. "Archaeal Communities in High Arctic Wetlands at Spitsbergen, Norway (78°N) as Characterized by 16S RRNA

- Gene Fingerprinting.” *FEMS Microbiology Ecology* 53 (1): 89–101.
<https://doi.org/10.1016/j.femsec.2005.01.004>.
- HOLLAND, HEINRICH D. 1984. *The Chemical Evolution of the Atmosphere and Oceans*. Princeton University Press. <https://doi.org/10.2307/j.ctv15r58kg>.
- Hönisch, Bärbel, N. Gary Hemming, David Archer, Mark Siddall, and Jerry F. McManus. 2009. “Atmospheric Carbon Dioxide Concentration across the Mid-Pleistocene Transition.” *Science* 324 (5934): 1551–54. <https://doi.org/10.1126/science.1171477>.
- Hugelius, G., J. Strauss, S. Zubrzycki, J. W. Harden, E. A.G. Schuur, C. L. Ping, L. Schirmer, et al. 2014. “Estimated Stocks of Circumpolar Permafrost Carbon with Quantified Uncertainty Ranges and Identified Data Gaps.” *Biogeosciences* 11 (23): 6573–93. <https://doi.org/10.5194/bg-11-6573-2014>.
- Ikeda-Fukazawa, Tomoko, Kenji Fukumizu, Kenji Kawamura, Shuji Aoki, Takakiyo Nakazawa, and Takeo Hondoh. 2005. “Effects of Molecular Diffusion on Trapped Gas Composition in Polar Ice Cores.” *Earth and Planetary Science Letters* 229 (3–4): 183–92. <https://doi.org/10.1016/j.epsl.2004.11.011>.
- Ikeda-Fukazawa, Tomoko, Shinichiro Horikawa, Takeo Hondoh, and Katsuyuki Kawamura. 2002. “Molecular Dynamics Studies of Molecular Diffusion in Ice Ih.” *Journal of Chemical Physics* 117 (8): 3886–96. <https://doi.org/10.1063/1.1495844>.
- Ikeda-Fukazawa, Tomoko, Katsuyuki Kawamura, and Takeo Hondoh. 2004. “Mechanism of Molecular Diffusion in Ice Crystals.” *Molecular Simulation* 30 (13–15): 973–79. <https://doi.org/10.1080/08927020410001709307>.
- Jongejans, Loeka L., Kai Mangelsdorf, Cornelia Karger, Thomas Opel, Sebastian Wetterich, Jérémy Courtin, Hanno Meyer, et al. 2022. “Molecular Biomarkers in Batagay Megaslump Permafrost Deposits Reveal Clear Differences in Organic Matter Preservation between Glacial and Interglacial Periods.” *Cryosphere* 16 (9): 3601–17. <https://doi.org/10.5194/tc-16-3601-2022>.
- Katayama, Taiki, Michiko Tanaka, Jun Moriiizumi, Toshio Nakamura, Anatoli Brouchkov, Thomas A. Douglas, Masami Fukuda, Fusao Tomita, and Kozo Asano. 2007. “Phylogenetic Analysis of Bacteria Preserved in a Permafrost Ice Wedge for 25,000 Years.” *Applied and Environmental Microbiology* 73 (7): 2360–63. <https://doi.org/10.1128/AEM.01715-06>.
- Kawagucci, Shinsuke, Urumo Tsunogai, Shingo Kudo, Fumiko Nakagawa, Hideyuki Honda, Shuji Aoki, Takakiyo Nakazawa, and Toshitaka Gamo. 2005. “An Analytical System for Determining $\Delta^{17}O$ in CO₂ Using Continuous Flow-Isotope Ratio MS.” *Analytical Chemistry* 77 (14): 4509–14. <https://doi.org/10.1021/ac050266u>.
- Khalil, K., B. Mary, and P. Renault. 2004. “Nitrous Oxide Production by Nitrification and Denitrification in Soil Aggregates as Affected by O₂ Concentration.” *Soil Biology and Biochemistry* 36 (4): 687–99. <https://doi.org/10.1016/j.soilbio.2004.01.004>.
- Kim, Kitae, Jinjung Ju, Bomi Kim, Hyun Young Chung, L’Ubica Vetráková, Dominik Heger, Alfonso Saiz-Lopez, Wonyong Choi, and Jungwon Kim. 2019. “Nitrite-Induced Activation of Iodate into Molecular Iodine in Frozen Solution.” *Environmental Science and Technology* 53 (9): 4892–4900. <https://doi.org/10.1021/acs.est.8b06638>.
- Kim, Kyungmin, Ji Woong Yang, Hyunsuk Yoon, Eunji Byun, Alexander Fedorov, Yeongjun Ryu, and Jinho Ahn. 2019. “Greenhouse Gas Formation in Ice Wedges at Cuyie, Central Yakutia.” *Permafrost and Periglacial Processes* 30 (1): 48–57. <https://doi.org/10.1002/ppp.1994>.
- Kizyakov, Alexander I., Sebastian Wetterich, Frank Günther, Thomas Opel, Loeka L. Jongejans, Jérémy Courtin, Hanno Meyer, et al. 2023. “Landforms and Degradation Pattern of the Batagay Thaw Slump, Northeastern Siberia.” *Geomorphology* 420 (October 2022). <https://doi.org/10.1016/j.geomorph.2022.108501>.
- Klüber, H. Detlef, and Ralf Conrad. 1998. “Inhibitory Effects of Nitrate, Nitrite, NO and N₂O on Methanogenesis by Methanosarcina Barkeri and Methanobacterium Bryantii.” *FEMS Microbiology Ecology* 25 (4): 331–39.

- [https://doi.org/10.1016/S0168-6496\(97\)00102-5](https://doi.org/10.1016/S0168-6496(97)00102-5).
- Kolhe, Parag, Elizabeth Amend, and Satish K. Singh. 2010. "Impact of Freezing on PH of Buffered Solutions and Consequences for Monoclonal Antibody Aggregation." *Biotechnology Progress* 26 (3): 727–33. <https://doi.org/10.1002/btpr.377>.
- Lachniet, Matthew S., Daniel E. Lawson, and Alison R. Sloat. 2012. "Revised 14C Dating of Ice Wedge Growth in Interior Alaska (USA) to MIS 2 Reveals Cold Paleoclimate and Carbon Recycling in Ancient Permafrost Terrain." *Quaternary Research (United States)* 78 (2): 217–25. <https://doi.org/10.1016/j.yqres.2012.05.007>.
- Land, Lynton S. 1980. "The Isotopic and Trace Element Geochemistry of Dolomite: The State of the Art." Edited by Donald H Zenger, John B Dunham, and Raymond L Ethington. *Concepts and Models of Dolomitization*. SEPM Society for Sedimentary Geology. <https://doi.org/10.2110/pec.80.28.0087>.
- Le, Nhat Thi Hong, Jinjung Ju, Bomi Kim, Min Sik Kim, Changha Lee, Saewung Kim, Wonyong Choi, Kitae Kim, and Jungwon Kim. 2020. "Freezing-Enhanced Non-Radical Oxidation of Organic Pollutants by Peroxymonosulfate." *Chemical Engineering Journal* 388 (January): 124226. <https://doi.org/10.1016/j.cej.2020.124226>.
- Liljedahl, Anna K., Julia Boike, Ronald P. Daanen, Alexander N. Fedorov, Gerald V. Frost, Guido Grosse, Larry D. Hinzman, et al. 2016. "Pan-Arctic Ice-Wedge Degradation in Warming Permafrost and Its Influence on Tundra Hydrology." *Nature Geoscience* 9 (4): 312–18. <https://doi.org/10.1038/ngeo2674>.
- Lim, Artem G., Sergey V. Loiko, Daria M. Kuzmina, Ivan V. Krickov, Liudmila S. Shirokova, Sergey P. Kulizhsky, Sergey N. Vorobyev, and Oleg S. Pokrovsky. 2021. "Dispersed Ground Ice of Permafrost Peatlands: Potential Unaccounted Carbon, Nutrient and Metal Sources." *Chemosphere* 266: 128953. <https://doi.org/10.1016/j.chemosphere.2020.128953>.
- Loulergue, Laetitia, Adrian Schilt, Renato Spahni, Valérie Masson-Delmotte, Thomas Blunier, Bénédicte Lemieux, Jean Marc Barnola, Dominique Raynaud, Thomas F. Stocker, and Jérôme Chappellaz. 2008. "Orbital and Millennial-Scale Features of Atmospheric CH₄ over the Past 800,000 Years." *Nature* 453 (7193): 383–86. <https://doi.org/10.1038/nature06950>.
- Lüthi, Dieter, Martine Le Floch, Bernhard Bereiter, Thomas Blunier, Jean Marc Barnola, Urs Siegenthaler, Dominique Raynaud, et al. 2008. "High-Resolution Carbon Dioxide Concentration Record 650,000-800,000 Years before Present." *Nature* 453 (7193): 379–82. <https://doi.org/10.1038/nature06949>.
- McGlynn, Shawn E., Grayson L. Chadwick, Christopher P. Kempes, and Victoria J. Orphan. 2015. "Single Cell Activity Reveals Direct Electron Transfer in Methanotrophic Consortia." *Nature* 526 (7574): 531–35. <https://doi.org/10.1038/nature15512>.
- Meyer, Hanno, Alexander Dereviagin, Christine Siegert, Lutz Schirrmeister, and Hans W. Hubberten. 2002. "Palaeoclimate Reconstruction on Big Lyakhovsky Island, North Siberia - Hydrogen and Oxygen Isotopes in Ice Wedges." *Permafrost and Periglacial Processes* 13 (2): 91–105. <https://doi.org/10.1002/ppp.416>.
- Midwood, A. J., and T. W. Boutton. 1998. "Soil Carbonate Decomposition by Acid Has Little Effect on $\Delta^{13}\text{C}$ of Organic Matter." *Soil Biology and Biochemistry* 30 (10–11): 1301–7. [https://doi.org/10.1016/S0038-0717\(98\)00030-3](https://doi.org/10.1016/S0038-0717(98)00030-3).
- Murray, Alison E., Fabien Kenig, Christian H. Fritsen, Christopher P. McKay, Kaelin M. Cawley, Ross Edwards, Emanuele Kuhn, et al. 2012. "Microbial Life at -13°C in the Brine of an Ice-Sealed Antarctic Lake." *Proceedings of the National Academy of Sciences of the United States of America* 109 (50): 20626–31. <https://doi.org/10.1073/pnas.1208607109>.
- Murton, Julian B., Thomas Opel, Phillip Toms, Alexander Blinov, Margret Fuchs, Jamie Wood, Andreas Gärtner, et al. 2022. "A Multimethod Dating Study of Ancient Permafrost, Batagay Megaslump, East Siberia." *Quaternary Research (United States)*

- 105: 1–22. <https://doi.org/10.1017/qua.2021.27>.
- Murton, Julian B, Mary E Edwards, Anatoly V Lozhkin, Patricia M Anderson, Grigoriy N Savvinov, Nadezhda Bakulina, Olesya V Bondarenko, et al. 2017. “Preliminary Paleoenvironmental Analysis of Permafrost Deposits at Batagaika Megaslump, Yana Uplands, Northeast Siberia” 87: 314–30. <https://doi.org/10.1017/qua.2016.15>.
- Murton, Julian, Thomas Opel, Sebastian Wetterich, Kseniia Ashastina, Grigoriy Savvinov, Petr Danilov, and Vasily Boeskorov. 2023. “Batagay Megaslump: A Review of the Permafrost Deposits, Quaternary Environmental History, and Recent Development.” *Permafrost and Periglacial Processes*. <https://doi.org/10.1002/ppp.2194>.
- Nikrad, Mrinalini P., Lee J. Kerkhof, and Max M. Häggblom. 2016. “The Subzero Microbiome: Microbial Activity in Frozen and Thawing Soils.” *FEMS Microbiology Ecology* 92 (6): 1–16. <https://doi.org/10.1093/femsec/fiw081>.
- Opel, Thomas, Alexander Yu Dereviagin, Hanno Meyer, Lutz Schirrmeister, and Sebastian Wetterich. 2011. “Palaeoclimatic Information from Stable Water Isotopes of Holocene Ice Wedges on the Dmitrii Laptev Strait, Northeast Siberia, Russia.” *Permafrost and Periglacial Processes* 22 (1): 84–100. <https://doi.org/10.1002/ppp.667>.
- Opel, Thomas, Hanno Meyer, Sebastian Wetterich, Thomas Laepple, Alexander Dereviagin, and Julian Murton. 2018. “Ice Wedges as Archives of Winter Paleoclimate: A Review.” *Permafrost and Periglacial Processes* 29 (3): 199–209. <https://doi.org/10.1002/ppp.1980>.
- Opel, Thomas, Julian B. Murton, Sebastian Wetterich, Hanno Meyer, Kseniia Ashastina, Frank Günther, Hendrik Grotheer, et al. 2019. “Past Climate and Continentality Inferred from Ice Wedges at Batagay Megaslump in the Northern Hemisphere’s Most Continental Region, Yana Highlands, Interior Yakutia.” *Climate of the Past* 15 (4): 1443–61. <https://doi.org/10.5194/cp-15-1443-2019>.
- Öquist, Mats G., Mats Nilsson, Fred Sörensson, Åsa Kasimir-Klemedtsson, Tryggve Persson, Per Weslien, and Leif Klemedtsson. 2004. “Nitrous Oxide Production in a Forest Soil at Low Temperatures - Processes and Environmental Controls.” *FEMS Microbiology Ecology* 49 (3): 371–78. <https://doi.org/10.1016/j.femsec.2004.04.006>.
- Ostrom, N. E., H. Gandhi, G. Trubl, and A. E. Murray. 2016. “Chemodenitrification in the Cryoecosystem of Lake Vida, Victoria Valley, Antarctica.” *Geobiology* 14 (6): 575–87. <https://doi.org/10.1111/gbi.12190>.
- Ostrom, Nathaniel E., Robin Sutka, Peggy H. Ostrom, A. Stuart Grandy, Kristin M. Huizinga, Hasand Gandhi, Joseph C. von Fischer, and G. Philip Robertson. 2010. “Isotopologue Data Reveal Bacterial Denitrification as the Primary Source of N₂O during a High Flux Event Following Cultivation of a Native Temperate Grassland.” *Soil Biology and Biochemistry* 42 (3): 499–506. <https://doi.org/10.1016/j.soilbio.2009.12.003>.
- Oyabu, Ikumi, Kenji Kawamura, Tsutomu Uchida, Shuji Fujita, Kyotaro Kitamura, Motohiro Hirabayashi, Shuji Aoki, et al. 2021. “Fractionation of O₂ and Ar₂ in the Antarctic Ice Sheet during Bubble Formation and Bubble-Clathrate Hydrate Transition from Precise Gas Measurements of the Dome Fuji Ice Core.” *The Cryosphere Discussions*, 1–45. <https://doi.org/10.5194/tc-2021-147>.
- Papina, T. S., N. S. Malygina, A. N. Eirikh, A. A. Galanin, and M. N. Zheleznyak. 2017. “Isotopic Composition and Sources of Atmospheric Precipitation in Central Yakutia.” *Earth’s Cryosphere* 21 (2): 60–69. [https://doi.org/10.21782/KZ1560-7496-2017-2\(60-69\)](https://doi.org/10.21782/KZ1560-7496-2017-2(60-69)).
- Picardal, Flynn. 2012. “Abiotic and Microbial Interactions during Anaerobic Transformations of Fe(II) and NO_x-.” *Frontiers in Microbiology* 3 (MAR): 1–7. <https://doi.org/10.3389/fmicb.2012.00112>.
- Pörtner, H, DC Roberts, and V Masson-Delmotte. 2022. *Summary for Policymakers*:

- Climate Change 2022_ Impacts, Adaptation and Vulnerability_Working Group II Contribution to the Sixth Assessment Report of the Intergovernmental Panel on Climate Change. Working Group II Contribution to the Sixth Assessment Report of the Intergovernmental Panel on Climate Change.*
<https://doi.org/10.1017/9781009325844>. Front.
- Prosser, James I., Linda Hink, Cécile Gubry-Rangin, and Graeme W. Nicol. 2020. “Nitrous Oxide Production by Ammonia Oxidizers: Physiological Diversity, Niche Differentiation and Potential Mitigation Strategies.” *Global Change Biology* 26 (1): 103–18. <https://doi.org/10.1111/gcb.14877>.
- Rivkina, Elizaveta, Viktoria Shcherbakova, Kestas Laurinavichius, Lada Petrovskaya, Kirill Krivushin, Gleb Kraev, Svetlana Pecheritsina, and David Gilichinsky. 2007. “Biogeochemistry of Methane and Methanogenic Archaea in Permafrost.” *FEMS Microbiology Ecology* 61 (1): 1–15. <https://doi.org/10.1111/j.1574-6941.2007.00315.x>.
- Rubino, M., D. M. Etheridge, C. M. Trudinger, C. E. Allison, M. O. Battle, R. L. Langenfelds, L. P. Steele, et al. 2013. “A Revised 1000 Year Atmospheric $\Delta^{13}\text{C-CO}_2$ Record from Law Dome and South Pole, Antarctica.” *Journal of Geophysical Research Atmospheres* 118 (15): 8482–99. <https://doi.org/10.1002/jgrd.50668>.
- Ryu, Yeongjun, Jinho Ahn, and Ji Woong Yang. 2018. “High-Precision Measurement of N_2O Concentration in Ice Cores.” *Environmental Science and Technology* 52 (2): 731–38. <https://doi.org/10.1021/acs.est.7b05250>.
- Salmon, Verity G., Christina Schädel, Rosvel Bracho, Elaine Pegoraro, Gerardo Celis, Marguerite Mauritz, Michelle C. Mack, and Edward A.G. Schuur. 2018. “Adding Depth to Our Understanding of Nitrogen Dynamics in Permafrost Soils.” *Journal of Geophysical Research: Biogeosciences* 123 (8): 2497–2512. <https://doi.org/10.1029/2018JG004518>.
- Schilt, Adrian, Matthias Baumgartner, Thomas Blunier, Jakob Schwander, Renato Spahni, Hubertus Fischer, and Thomas F. Stocker. 2010. “Glacial-Interglacial and Millennial-Scale Variations in the Atmospheric Nitrous Oxide Concentration during the Last 800,000 Years.” *Quaternary Science Reviews* 29 (1–2): 182–92. <https://doi.org/10.1016/j.quascirev.2009.03.011>.
- St-Jean, Mélanie, Bernard Lauriol, Ian D. Clark, Denis Lacelle, and Christian Zdanowicz. 2011. “Investigation of Ice-Wedge Infilling Processes Using Stable Oxygen and Hydrogen Isotopes, Crystallography and Occluded Gases (O_2 , N_2 , Ar).” *Permafrost and Periglacial Processes* 22 (1): 49–64. <https://doi.org/10.1002/ppp.680>.
- Teepe, R., R. Brumme, and F. Beese. 2001. “Nitrous Oxide Emissions from Soil during Freezing and Thawing Periods.” *Soil Biology and Biochemistry* 33 (9): 1269–75. [https://doi.org/10.1016/S0038-0717\(01\)00084-0](https://doi.org/10.1016/S0038-0717(01)00084-0).
- Tiedje, James M. 1988. “Ecology of Denitrification and Dissimilatory Nitrate Reduction to Ammonium.” *Environmental Microbiology of Anaerobes*, no. April: 179–244.
- Tsunogai, Urumu, Fumiko Nakagawa, Fumiko Nakagawa, and Yosuke Hachisu. 2000. “Stable Carbon and Oxygen Isotopic Analysis of Carbon Monoxide in Natural Waters.” *Rapid Communications in Mass Spectrometry* 14 (16): 1507–12. [https://doi.org/10.1002/1097-0231\(20000830\)14:16<1507::AID-RCM56>3.0.CO;2-E](https://doi.org/10.1002/1097-0231(20000830)14:16<1507::AID-RCM56>3.0.CO;2-E).
- Vasil’chuk, Yu K. 1991. “Reconstruction of the Paleoclimate of the Late Pleistocene and Holocene on the Basis of Isotope Studies of Subsurface Ice and Waters of the Permafrost Zone.” *Water Resources* 17 (6): 640–47.
- Vasil’chuk, Yuriy K., Nadine A. Budantseva, Alla C. Vasil’chuk, and Julia N. Chizhova. 2020. “Winter Air Temperature during the Holocene Optimum in the North-Eastern Part of the East European Plain Based on Ice Wedge Stable Isotope Records.” *Permafrost and Periglacial Processes* 31 (2): 281–95. <https://doi.org/10.1002/ppp.2043>.
- Voigt, Carolina, Maija E. Marushchak, Benjamin W. Abbott, Christina Biasi, Bo Elberling, Steven D. Siciliano, Oliver Sonntag, Katherine J. Stewart, Yuanhe Yang, and Pertti

- J. Martikainen. 2020. "Nitrous Oxide Emissions from Permafrost-Affected Soils." *Nature Reviews Earth and Environment* 1 (8): 420–34. <https://doi.org/10.1038/s43017-020-0063-9>.
- Wetterich, S., H. Meyer, M. Fritz, G. Mollenhauer, J. Rethemeyer, A. Kizyakov, L. Schirrmeister, and T. Opel. 2021. "Northeast Siberian Permafrost Ice-Wedge Stable Isotopes Depict Pronounced Last Glacial Maximum Winter Cooling." *Geophysical Research Letters* 48 (7). <https://doi.org/10.1029/2020GL092087>.
- Whiticar, Michael J. 1999. "Carbon and Hydrogen Isotope Systematics of Bacterial Formation and Oxidation of Methane." *Chemical Geology* 161 (1): 291–314. [https://doi.org/10.1016/S0009-2541\(99\)00092-3](https://doi.org/10.1016/S0009-2541(99)00092-3).
- Wilhelm, Roland C., Kristin J. Radtke, Nadia C.S. Mykityczuk, Charles W. Greer, and Lyle G. Whyte. 2012. "Life at the Wedge: The Activity and Diversity of Arctic Ice Wedge Microbial Communities." *Astrobiology* 12 (4): 347–60. <https://doi.org/10.1089/ast.2011.0730>.
- Yang, Ji-Woong, Jinho Ahn, Edward Brook, and Yeongjun Ryu. 2017. "Atmospheric Methane Control Mechanisms during the Early Holocene." *Climate of the Past Discussions* 4: 1–22. <https://doi.org/10.5194/cp-2016-75>.
- Yang, Ji-Woong, Jinho Ahn, Go Iwahana, Nayeon Ko, Ji-Hoon Kim, Kyungmin Kim, Alexander Fedorov, and Sangyoung Han. 2022. "Origin of CO₂, CH₄, and N₂O Trapped in Ice Wedges in Central Yakutia and Their Relationship." *Permafrost and Periglacial Processes*, no. September: 1–20. <https://doi.org/10.1002/ppp.2176>.
- Yang, Ji Woong, Jinho Ahn, Go Iwahana, Sangyoung Han, Kyungmin Kim, and Alexander Fedorov. 2020. "Brief Communication: The Reliability of Gas Extraction Techniques for Analysing CH₄ and N₂O Compositions in Gas Trapped in Permafrost Ice Wedges." *Cryosphere* 14 (4): 1311–24. <https://doi.org/10.5194/tc-14-1311-2020>.
- Yi, Yoo Soo, Yeongcheol Han, Kideok D. Kwon, Sung Keun Lee, and Soon Do Hur. 2021. "Molecular Mechanism of Gas Diffusion in Ice-Ih." *ACS Earth and Space Chemistry* 5 (11): 3258–67. <https://doi.org/10.1021/acsearthspacechem.1c00308>.
- Zhu, Xia, Martin Burger, Timothy A. Doane, and William R. Horwath. 2013. "Ammonia Oxidation Pathways and Nitrifier Denitrification Are Significant Sources of N₂O and NO under Low Oxygen Availability." *Proceedings of the National Academy of Sciences of the United States of America* 110 (16): 6328–33. <https://doi.org/10.1073/pnas.1219993110>.

Abstract in Korean

국문초록

영구동토층은 미래의 지구 온난화 상황에서 온실 가스(GHGs)의 중요한 원천이 될 수 있다. 그러나 영구동토층 지역에서의 온실가스의 형성 메커니즘은 잘 이해되지 않고 있다. 영구동토 지역에서 흔히 볼 수 있는 얼음 썩기에는 매우 높은 농도의 온실기체를 함유한 버블이 포함되어 있으며, 이 가스 버블 내의 온실기체 분석을 통해 영구동토 지역, 특히 영하의 온도에서 온실기체 형성 메커니즘을 더 잘 이해할 것이라 기대한다. 우리는 북동시베리아 야쿠시아(Yakutia)의 야나(Yana) 고원에 위치한 세계에서 가장 큰 해동 슬럼프인 바타가이 메가슬럼프의 상부 얼음 복합체(UIC)와 하부 얼음 복합체(LIC)에서 얼음썩기 샘플을 사용하여 온실기체 농도 분석을 진행하였다. 우리는 가스 버블의 Ar/N₂/O₂ 조성과 얼음의 물동위원소 비율 ($\delta^{18}\text{O}$ 및 δD)을 분석하여 얼음 썩기 형성 과정을 추정하였다. 그런 다음, 이산화탄소와 메탄의 탄소 안정 동위원소와 얼음 썩기에 포함된 퇴적 입자, 온실기체의 혼합 비율과 이온 조성 간의 관계를 분석함으로써 얼음 썩기 내부 온실기체의 기원과 형성 메커니즘을 제안하였다. 연구 지역의 얼음 썩기는 건조한 눈이나 서리가 압착되어 형성되었을 것으로 보이며, 얼음 썩기 형성 이후에도 미생물 활동이 존재하여 온실기체를 형성하였을 것으로 보인다. 특히, 아산화질소의 경우, 혼합 비율이 LIC에서 더 적었는데, 이러한 결과는 미생물 군집의 차이가 있었기 때문으로 보인다. 이러한 결과는 얼음썩기 내에서 온실기체 형성이 물리화학적 조건뿐만 아니라 미생물 활동과 환경 조건 사이의 복잡한 상호작용을 포함한다는 것을 시사한다.

List of Figures

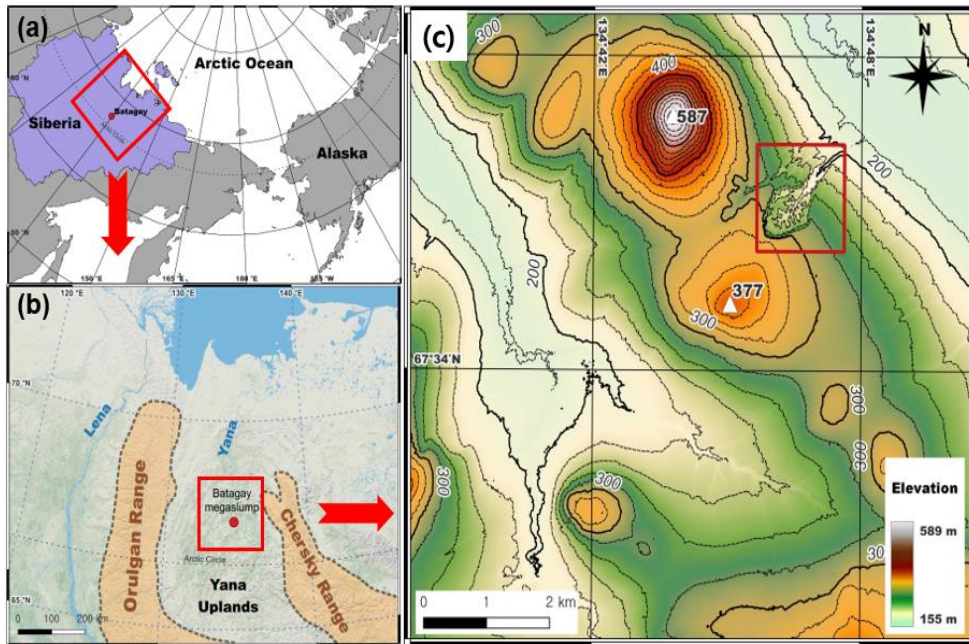


Figure 1. (a) Location map of Batagay and the Arctic Ocean. Red box indicates location of panel b. (b) Location map showing Batagay megaslump within the Yana River basin in northern Yakutia. Shaded and dashed orange lines depict two ranges surrounding the Yana Uplands. Red box indicates location of panel c. (c) Topographic map of Batagay megaslump (red box), illustrating its position on a northeast-facing hillslope.

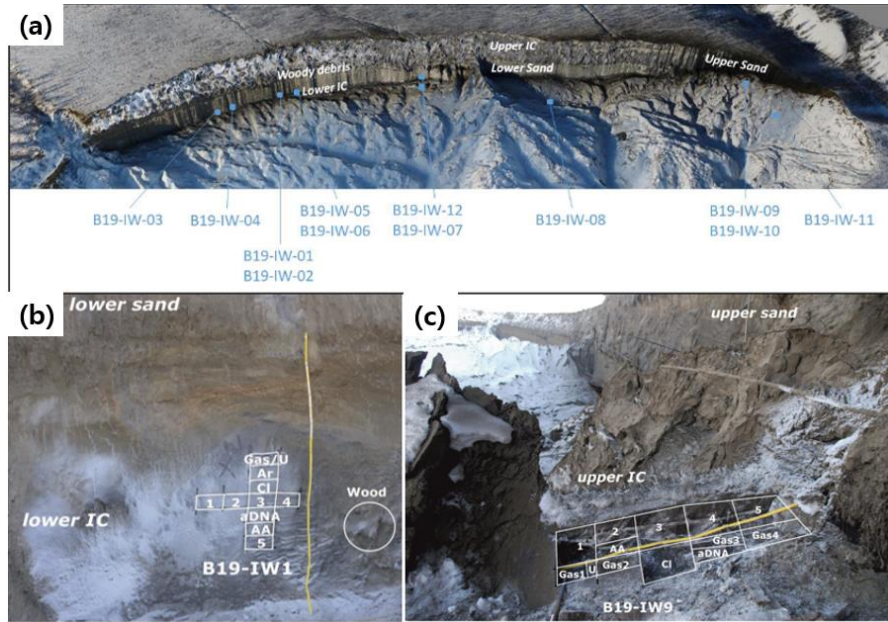


Figure 2. Headwall of the Batagay megaslump with approximate sampling positions (A). One of the Lower Ice Complex's ice wedge, B19-IW1 (B), Upper Ice Complex's ice wedge, B19-IW9 (C).

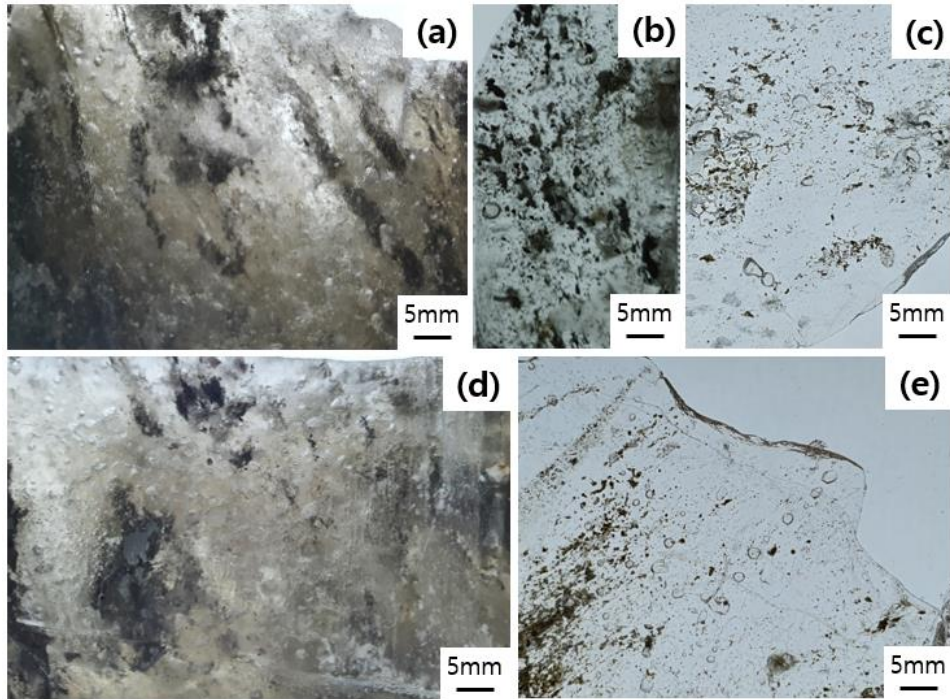


Figure 3. Photographs of ice wedge blocks (a, d) and Microphotographs (b, c, e) of ice wedge thin sections from Batagay megaslump. (a,b,c) from UIC and (d, e) from LIC. Generally, spherical air bubbles (averaging 2 mm in diameter) are observed in most areas and it is respect with low melting of ice.

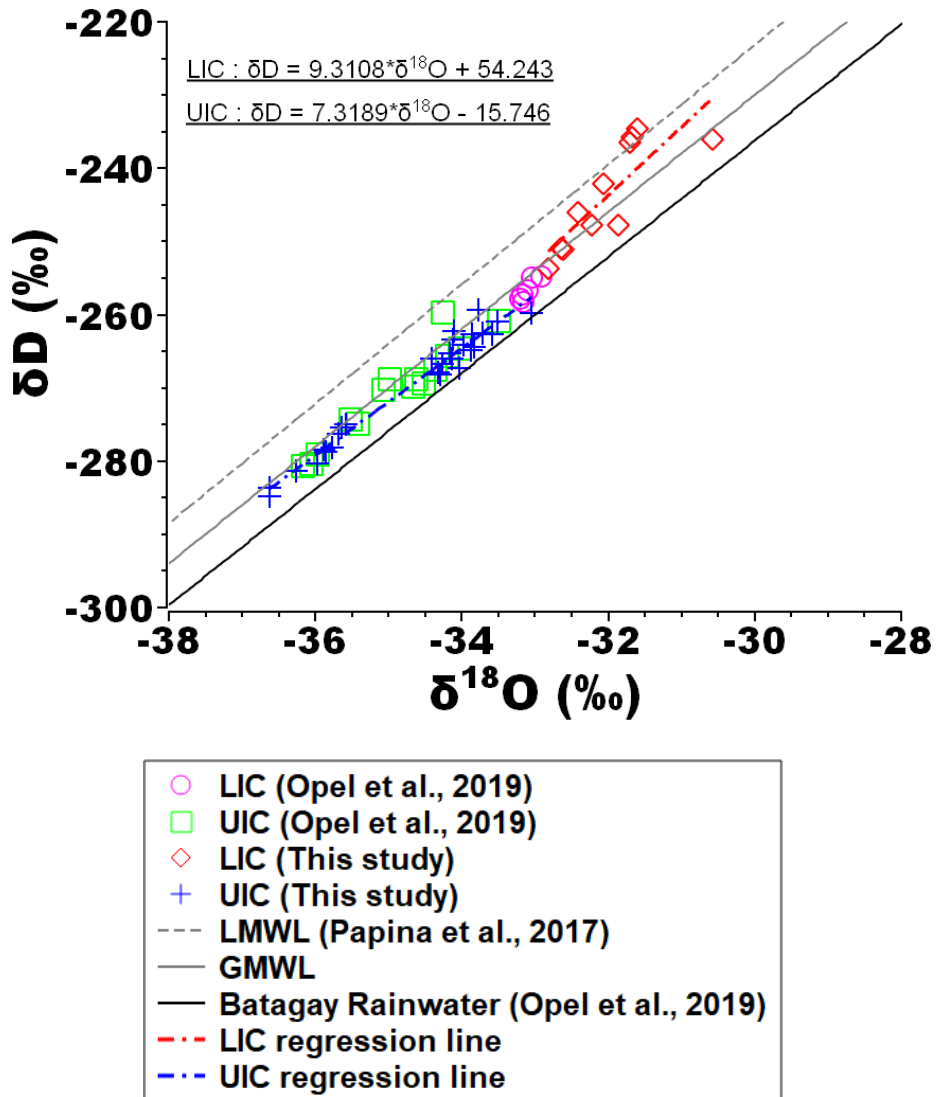


Figure 4. Dual water stable isotope diagram for Batagay ice wedges. Global Meteoric Water Line (GMWL) is indicated by $\delta D = 8 \times \delta^{18}O + 10$ and Local Meteoric Water Line (LMWL for Yakutsk, 600 km south of Batagay) is indicated by $\delta D = 8.177.3198 \times \delta^{18}O + -21.9415.746$, based on Papina et al.(Papina et al. 2017) Batagay rainwater (n=4) is indicated by $\delta D = 7.93 \times \delta^{18}O - 1.65$ based on Opel et al.(Opel et al. 2019) Dash-dotted red and blue lines are regression lines for LIC and UIC, respectively.

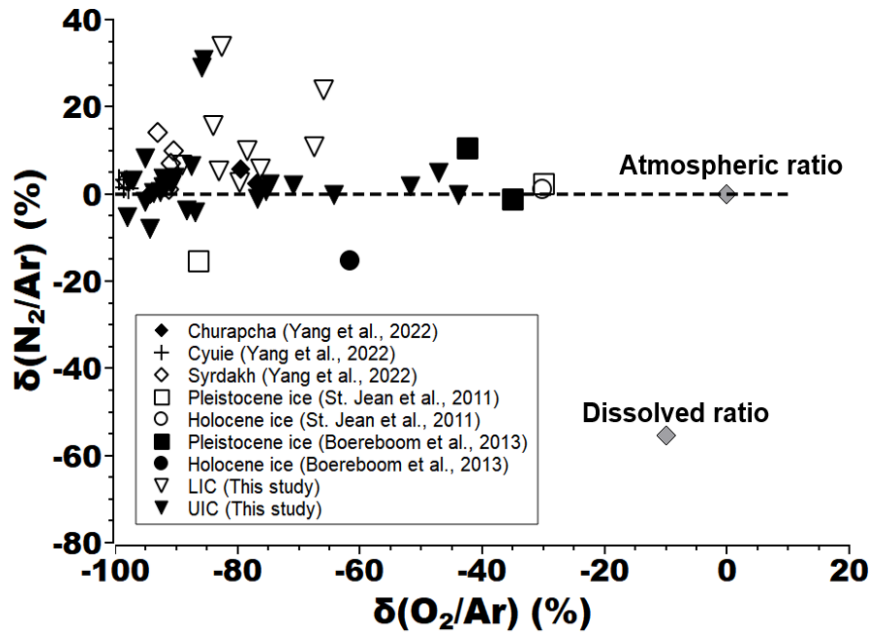


Figure 5 $\delta(\text{N}_2/\text{Ar})$ and $\delta(\text{O}_2/\text{Ar})$ mixing ratios of various ice wedges corresponding to different locations and ages. Shaded gray and outlined black diamonds reflect atmospheric ratio or each gas completely dissolved in liquid water, respectively. Unfilled or filled lower triangles indicate Batagay LIC and UIC, respectively. Other symbols represent ice wedge values in the Yakutsk region in Central Siberia formed in the Last Glacial Periods (Yang et al., 2022), those near the Labtev sea region formed in the Pleistocene and Holocene (Boereboom et al., 2013), and those in the Alaska region formed in the Pleistocene and Holocene (St. Jean et al., 2011).

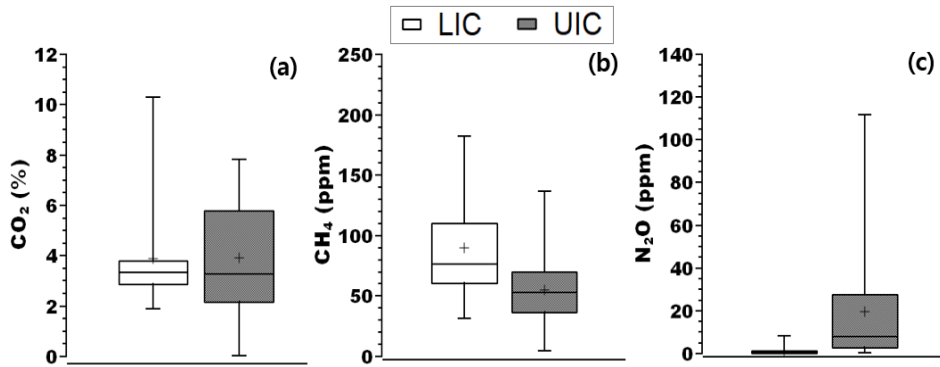


Figure 6. Greenhouse gas mixing ratios in ice wedges of the Batagay megaslump. The box represents the interquartile range, with the bottom and top indicating the 25th and 75th percentiles, respectively. The horizontal line within the box represents the median value, whereas the “+” symbol denotes the mean. Whiskers extending from each end of the box represent minimum and maximum values of the data points.

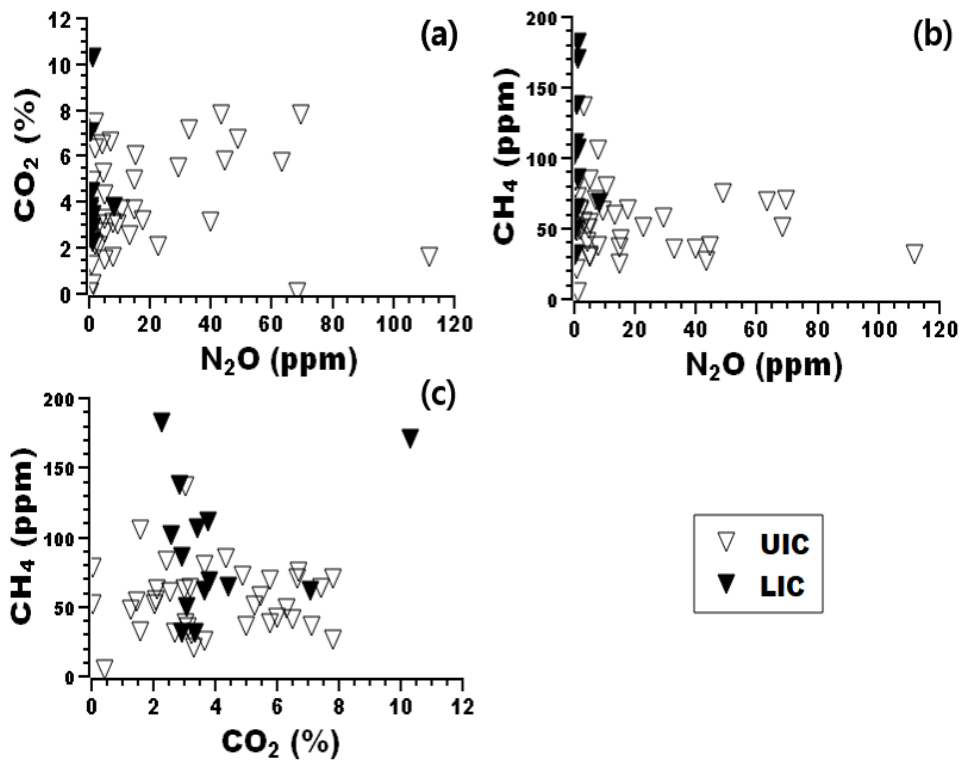


Figure 7. Correlation plot of greenhouse gas mixing ratios in Batagay ice wedges for UIC and LIC units. (a) CH₄ vs. CO₂, (b) N₂O vs. CH₄, (c) CO₂ vs. CH₄. Each gas mixing ratio was measured simultaneously in the same extracted gas at the LIC and UIC. Unfilled and filled lower triangles represent data from UIC and LIC, respectively.

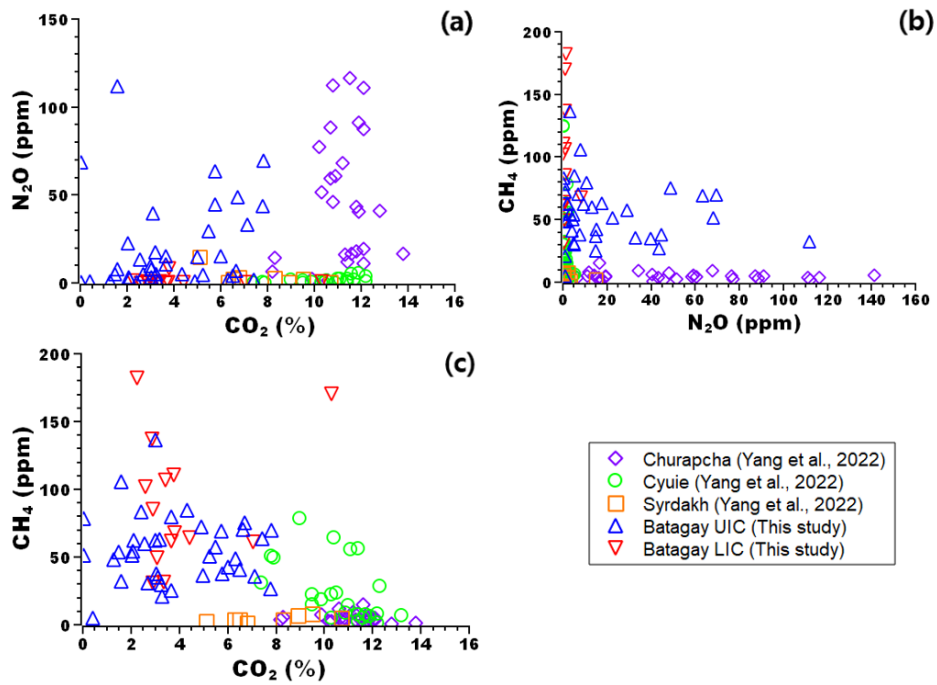


Figure 8. Correlation plots of greenhouse gas relationships in ice wedges from different ages and locations in Siberia. (a) N₂O vs. CO₂. (b) CH₄ vs. N₂O. (c) CH₄ vs. CO₂. Data were obtained from different ice wedges and locations in Siberia (Yang et al., 2022)

List of Tables

Table 1 Gas composition (CO₂, CH₄, N₂O, Ar, O₂, and N₂), air contents, water stable isotopes, soil contents, and soil chemistry for LIC and UIC layers.

Parameter	Lower Ice Complex (B19-IW1, 3, 5)				Upper Ice Complex (B19-IW8, 9, 10, 11)			
	Mean	Max.	Min.	n	Mean	Max.	Min.	n
Ar (%)	0.95	1.04	0.76	9	1.07	1.20	0.87	26
O ₂ (%)	4.45	7.50	2.49	9	3.97	12.85	83.48	26
N ₂ (%)	89.63	95.18	79.30	9	92.00	98.77	83.48	26
N ₂ O (ppm)	1.16	8.16	0.12	14	19.45	111.88	0.30	38
CH ₄ (ppm)	90.08	182.04	31.17	14	54.97	136.42	4.76	38
CO ₂ (%)	3.88	10.30	1.88	15	3.90	7.82	0.03	38
Air contents (mL/g _{ice})	0.0101	0.0193	0.0034	10	0.0110	0.0218	0.0028	25
δ ¹⁸ O _{ice} (‰)	-32.02	-30.58	-32.82	11	-34.67	-33.05	-36.63	29
δD _{ice} (‰)	-	-	-	11	-	-	-	29
d-excess(‰)	12.27	18.14	7.22	11	7.87	10.96	4.64	29
Soil contents (g/g _{ice})	0.0136	0.0171	0.0083	4	0.0179	0.0592	0.0051	11
C (wt%)	0.74	0.99	0.54	5	1.17	1.52	1.00	5
N (wt%)	0.07	0.10	0.06	5	0.12	0.16	0.09	5
Soil δ ¹³ C	-25.80	-25.74	-25.96	5	-25.56	-25.36	-25.97	5
Soil δ ¹⁵ N	3.38	6.77	0.92	5	4.10	9.14	2.40	5
C/N	9.76	11.23	8.42	5	10.19	11.42	9.40	5

Table 2 GHG mixing ratios, Ar/O₂/N₂, δ(O₂/Ar) and δ(N₂/Ar) values from Batagay ice wedge measured using a dry and wet extraction technique.

Layer	Sample ID	Ar	O ₂	N ₂	δ(O ₂ /Ar)	δ(N ₂ /Ar)	N ₂ O (ppm)	CH ₄ (ppm)	CO ₂ (%)	Method	
Lower Ice Complex	B19-IW1-gas	1.01	2.49	89.99	-89.01	6.64	0.23	61.49	3.66	Wet	
		1.03	3.94	90.78	-82.97	5.26	0.51	61.20	7.06		
								0.99	85.38	2.91	Dry
								0.36	110.77	3.77	
								0.19	31.17	2.91	
	B19-IW3-gas	1.04	4.78	89.87	-79.65	2.66	0.57	49.36	3.08	Wet	
		0.76	5.21	79.30	-65.87	23.77	2.06	403.43	14.5986		
		1.02	5.49	90.92	-76.22	5.67	0.61	64.43	4.43		
								8.16	68.06	3.79	Dry
								0.25	31.35	3.35	
	B19-IW5-gas	0.96	3.48	93.44	-83.97	15.56	-	-	1.88	Wet	
		0.97	4.08	89.26	-78.36	9.85	1.24	182.04	2.2589		
		0.78	3.07	87.96	-82.60	33.86	1.05	106.63	3.42		
		1.02	7.50	95.18	-67.43	10.82	1.13	170.31	10.30		
								0.87	137.11	2.86	Dry
							0.12	101.87	2.58		

Upper Ice Complex	B19-IW8-gas1	1.07	0.69	92.92	-97.13	3.12	2.09	62.31	2.12	Wet
		1.17	1.51	90.16	-94.27	-8.06	0.92	979.82	8.89	
							0.30	78.44	0.03	Dry
							17.56	63.03	3.19	
						0.45	83.23	2.42		
	B19-IW8-gas2	0.87	2.78	94.31	-85.84	28.92	3.07	54.53	2.08	Wet
		0.90	2.94	98.77	-85.50	30.64	3.07	54.53	2.08	
		1.04	1.14	94.12	-95.10	8.20			3.56	
		1.11	3.13	98.63	-87.44	6.27	7.65	37.80	3.05	
							1.13	4.76	0.43	Dry
	B19-IW9-gas1	1.10	1.95	95.51	-92.11	3.43	3.20	136.42	3.02	Wet
		1.11	2.03	94.53	-90.77	1.83	10.68	79.52	3.6584	
		0.97	11.58	85.36	-47.06	4.75	0.96	48.10	1.27	
							0.94	20.88	3.30	Dry
	B19-IW9-gas2	1.09	8.83	91.54	-64.17	-0.36	22.68	51.34	2.05	Wet
		1.02	12.85	85.09	-43.85	-0.21	5.01	53.89	1.4752	
		1.09	2.37	94.82	-90.32	3.69	5.04	29.76	3.24	
							1.07	72.42	4.89	Dry
	B19-IW9-gas3	1.15	6.01	95.03	-76.71	-1.15	9.50	62.40	3.01	Wet
		1.11	1.81	94.13	-92.09	1.44	15.02	25.21	3.6685	
1.03		5.75	87.35	-75.34	0.58	14.78	36.46	4.99		

						4.93	30.96	2.68	Dry
B19-IW9-gas4	0.98	10.67	83.88	-51.76	1.74	39.77	35.16	3.12	Wet
	1.07	7.08	91.21	-70.81	1.88	111.88	32.17	1.5935	
	1.05	5.99	90.11	-74.71	2.15	13.21	60.01	2.54	
						7.85	105.72	1.59	Dry
B19-IW10-gas1	0.99	1.64	83.48	-92.65	0.29	44.58	37.71	5.77	Wet
	1.12	1.25	91.94	-95.02	-1.90	43.58	26.75	7.79	
						29.23	57.67	5.48	Dry
						32.99	35.74	7.13	
B19-IW10-gas2	1.05	1.93	89.67	-91.86	1.54	63.38	69.38	5.75	Wet
	1.11	1.58	92.87	-93.66	0.10	69.53	69.94	7.82	
						68.36	51.26	0.05	Dry
						48.86	75.14	6.71	
B19-IW11-gas1	1.17	3.09	94.88	-88.34	-3.82	15.22	42.32	6.00	Wet
	1.18	0.51	93.66	-98.07	-5.49	1.97	63.29	7.42	
						1.81	48.66	6.32	Dry
						5.27	84.79	4.33	
B19-IW11-gas2	1.20	3.56	96.33	-86.84	-4.36	6.90	70.64	6.65	Wet
	1.06	0.54	91.70	-97.76	2.88	4.50	50.39	5.25	
						4.17	40.81	6.50	Dry

Table 3. Major ion concentrations and pH from Batagay ice wedge meltwater samples measured at National Instrumentation Center for Environmental Management. "n.a." denotes data not applicable. "n.m." denotes data not measured.

9		Cl ⁻	NO ₃ ⁻	NH ₄ ⁺	NO ₂ ⁻	SO ₄ ²⁻	Ca ²⁺	Mg ²⁺	Na ⁺	K ⁺	Fe	pH
		mg/L	mg/L	mg/L	mg/L	mg/L	mg/L	mg/L	mg/L	mg/L	mg/L	μg/L
Lower Ice Complex	B19-IW1-gas	22.219	n.a.	3.574	n.m.	1.696	13.338	5.587	1.588	19.328	581.42	7.51
		22.3433	n.a.	3.984939	n.a.	2.0299	10.6424	4.956771	3.164975	21.42438	n.m.	n.m.
	B19-IW3-gas	6.136	n.a.	n.a.	n.m.	2.032	17.448	5.583	1.196	6.956	448.66	7.23
		6.82	n.a.	1.59559	n.a.	2.297	16.35247	5.754809	2.555657	7.598889	n.m.	n.m.
	B19-IW5-gas	2.605	n.a.	1.105	n.m.	1	8.399	3.479	n.a.	1.913	55.017	7.21
		3.448	n.a.	1.002	n.m.	1.008	9.546	4.652	1.013	3.169	292.89	7.43
4.106		9.2123	n.a.	n.a.	1.3915	9.790093	4.203909	2.517449	2.951867	552.55	7.36	
Upper Ice Complex	B19-IW8-gas1	4.284	n.a.	n.a.	n.m.	n.a.	21.125	8.003	1.342	5.535	8.835	7.41
	B19-IW8-gas2	2.973	n.a.	n.a.	n.m.	n.a.	20.736	6.02	1.389	3.396	12.794	7.43
	B19-IW9-gas1	5.2474	n.a.	1.275299	n.a.	5.2789	10.21926	4.146379	2.161805	2.822374	191.96	7.56
	B19-IW9-gas2	1.9431	n.a.	2.535427	1.49	1.9805	50.10762	20.95881	3.348837	8.118776	5.713	7.31
	B19-IW9-gas3	1.7386	n.a.	1.234158	n.a.	0.6	11.21968	3.638247	2.14455	2.881372	133.12	7.43
	B19-IW9-gas4	2.9053	10.0202	n.a.	n.a.	2.021	49.62763	13.1508	3.776448	5.592395	3.329	7.57
	B19-IW10-gas1	2.2971	n.a.	n.a.	1.75	0.9832	16.64973	3.871045	2.445932	3.917898	11.126	7.71
	B19-IW10-gas2	1.794	n.a.	n.a.	n.m.	n.a.	13.86	3.933	n.a.	3.625	18.332	7.53
2.0458		n.a.	n.a.	1.51	0.9777	13.25502	3.176137	2.208118	3.443052	n.m.	n.a.	

	B19-IW11-gas1	3.6033	n.a.	3.467607	n.a.	0.7728	14.37643	3.512146	2.329047	5.531155	n.m.	7.3
	B19-IW11-gas2	1.997	10.237	n.a.	n.m.	1.775	36.292	10.179	1.297	4.585	42.272	n.m.
		2.8884	n.a.	n.a.	n.a.	n.a.	15.00981	3.735384	2.312981	4.031102	n.m.	n.m.

Table 4. Stable water isotope ratio from Batagay ice wedge measured at Iwha Womans University in Korea.

Layer	Sample ID	$\delta^{18}\text{O}_{\text{VSMOW}}$ (‰)	$\delta^2\text{H}_{\text{VSMOW}}$ (‰)	d-excess (‰)
Lower Ice Complex	B19-IW1-gas	-32.41	-246.09	13.22
		-32.07	-242.16	14.38
		-30.58	-236.09	8.59
	B19-IW3-gas	-31.70	-236.51	17.05
		-31.60	-234.65	18.14
		-31.68	-235.81	17.61
	B19-IW5-gas	-32.82	-253.75	8.79
		-32.62	-251.04	9.92
		-31.87	-247.71	7.22
		-32.23	-247.80	10.01
Upper Ice Complex	B19-IW8-gas1	-32.64	-251.01	10.08
		-33.98	-264.19	7.68
		-33.86	-262.67	8.24
	B19-IW8-gas2	-34.17	-265.21	8.14
		-34.41	-266.03	9.27
		-34.11	-262.29	10.58
	B19-IW9-gas1	-33.78	-259.30	10.96
		-34.12	-263.33	9.66
B19-IW9-gas1	-34.30	-268.15	6.28	
	-34.26	-266.75	7.34	

		-34.33	-267.91	6.76
	B19-IW9-gas2	-34.30	-268.22	6.20
		-34.14	-266.07	7.07
		-33.59	-262.66	6.05
	B19-IW9-gas3	-33.88	-264.83	6.22
		-33.71	-262.55	7.14
		-33.51	-260.94	7.13
	B19-IW9-gas4	-34.03	-267.25	4.99
		-33.83	-264.35	6.29
		-33.05	-259.75	4.64
	B19-IW10-gas1	-36.63	-284.74	8.32
		-36.63	-283.67	9.39
		-36.26	-281.34	8.75
	B19-IW10-gas2	-35.86	-278.72	8.17
		-35.64	-275.45	9.67
		-35.68	-276.22	9.23
	B19-IW11-gas1	-35.98	-280.31	7.51
		-35.77	-278.16	8.01
	B19-IW11-gas2	-35.88	-278.38	8.64
		-35.59	-274.96	9.78

Table 5. Carbon isotope data and concentration of CO₂ and CH₄ measured by Nagoya University, Japan. "n.m." denotes data not measured.

Layer	Sample ID	Measurement	CO ₂ (%)	$\delta^{13}\text{C}-\text{CO}_2$ (‰)	CH ₄ (ppm)	$\delta^{13}\text{C}-\text{CH}_4$ (‰)
Lower Ice Complex	B19-IW1-gas	CO ₂ & CH ₄	3.3	-24.9	58	-47.3
		CO ₂	3.4	-22.2	n.m.	n.m.
	B19-IW3-gas	CO ₂	2.6	-21.5	n.m.	n.m.
		CH ₄	n.m.	n.m.	117	-48.9
Upper Ice Complex	B19-IW10-gas1	CO ₂	4.8	-24.1	n.m.	n.m.
		CH ₄	n.m.	n.m.	124	-36.7
	B19-IW11-gas1	CO ₂	3.7	-25.0	n.m.	n.m.
		CO ₂	3.5	-22.2	n.m.	n.m.

Table 6. Soil N,C,and H weight composition and C/N ratio, also carbon stable isotope and nitrogen stable isotope data from Batagay ice wedge samples measured at National Instrumentation Center for Environmental Management.

Layer	Sample ID	N (wt%)	C (wt%)	H (wt%)	C/N	$\delta^{13}\text{C}_{\text{PDB}}$ (‰)	$\delta^{15}\text{N}_{\text{AIR}}$ (‰)
Lower Ice Complex	B19-IW1-gas	0.0881	0.9891	0.3848	11.22701	-25.77	3.3
	B19-IW3-gas	0.1008	0.9542	0.3835	9.46627	-25.74	3.93
	B19-IW5-gas	0.0638	0.5372	0.3091	8.420063	-25.79	0.92
	B19-IW5-gas	0.0614	0.5514	0.2938	8.980456	-25.96	6.77
	B19-IW5-gas	0.0605	0.6482	0.2936	10.71405	-25.76	1.99
Upper Ice Complex	B19-IW8-gas1	0.1177	1.2175	0.3872	10.3441	-25.43	2.54
	B19-IW9-gas1	0.1621	1.5235	0.4249	9.398519	-25.36	3.69
	B19-IW9-gas2	0.0979	1.0159	0.3636	10.37692	-25.58	2.74
	B19-IW9-gas4	0.0878	1.0029	0.3486	11.42255	-25.97	2.4
	B19-IW10-gas1	0.1141	1.0737	0.3751	9.410167	-25.47	9.14

Table 7. Correlation table for major greenhouse gases (CO₂, CH₄, N₂O)

Parameter 1	Parameter 2		r	p-value
N ₂ O	CH ₄	LIC	0.0012	<0.001
		UIC	-0.14	<0.001
		ALL	-0.23	<0.001
N ₂ O	CO ₂	LIC	0.013	0.00127
		UIC	0.15	<0.001
		ALL	0.12	0.00136
CH ₄	CO ₂	LIC	0.24	<0.001
		UIC	-0.023	<0.001
		ALL	0.08	<0.001